



저작자표시-비영리-변경금지 2.0 대한민국

이용자는 아래의 조건을 따르는 경우에 한하여 자유롭게

- 이 저작물을 복제, 배포, 전송, 전시, 공연 및 방송할 수 있습니다.

다음과 같은 조건을 따라야 합니다:



저작자표시. 귀하는 원저작자를 표시하여야 합니다.



비영리. 귀하는 이 저작물을 영리 목적으로 이용할 수 없습니다.



변경금지. 귀하는 이 저작물을 개작, 변형 또는 가공할 수 없습니다.

- 귀하는, 이 저작물의 재이용이나 배포의 경우, 이 저작물에 적용된 이용허락조건을 명확하게 나타내어야 합니다.
- 저작권자로부터 별도의 허가를 받으면 이러한 조건들은 적용되지 않습니다.

저작권법에 따른 이용자의 권리는 위의 내용에 의하여 영향을 받지 않습니다.

이것은 [이용허락규약\(Legal Code\)](#)을 이해하기 쉽게 요약한 것입니다.

[Disclaimer](#)

Thesis for the Degree of Master of Science

Study of Geochemical Reaction for
Plagioclase, Orthoclase and Biotite under
Supercritical CO₂ – Water – Mineral
System at CO₂ Sequestration Sites



Wonwoo Choi

Department of Environmental Geosciences

The Graduate School

Pukyong National University

February, 2010

Study of Geochemical Reaction for
Plagioclase, Orthoclase and Biotite under
Supercritical CO₂ – Water – Mineral
System at CO₂ Sequestration Sites

이산화탄소 지중저장지에서 과임계이산화탄소와 물에
의한 사장석, 정장석 그리고 흑운모의
지화학적 반응 연구

Advisor: Minhee Lee

by

Wonwoo Choi

A thesis submitted in partial fulfillment of requirements
for the degree of Master of Science

in Department of Environmental Geosciences,
The Graduate School,
Pukyong National University

February, 2010

Study of Geochemical Reaction for Plagioclase, Orthoclase
and Biotite under Supercritical CO₂ – Water – Mineral
System at CO₂ Sequestration Sites

A Thesis
by
Wonwoo Choi

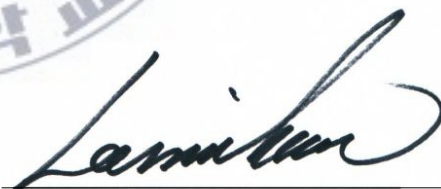
Approved as to style and content by :



(Chairman) Sookyun Wang



(Member) Deok-Heung Hwang



(Member) Minhee Lee

February 25, 2010

Study of Geochemical Reaction for Plagioclase, Orthoclase and Biotite
under Supercritical CO₂ – Water – Mineral System at CO₂
Sequestration Sites

Wonwoo Choi

*Department of Environmental Geosciences, Graduate School,
Pukyong National University, Republic of Korea*

Abstract

Laboratory scale experiments to quantify the geochemical reaction among the supercritical CO₂-typical silicate minerals-water occurred in the deep brine aquifer as the CO₂ sequestration site were performed in the high-pressurized cell. Polished mineral crystals such as plagioclase ([Ca, Na₂]O·Al₂O₃·2SiO₂), orthoclase (KAlSi₃O₈), and biotite (K[Mg, Fe]₃AlSi₃O₁₀(OH)₂) were fixed in the cell on geological sequestration conditions (100 bar and 50 °C) and each mineral crystal was reacted with the supercritical CO₂ for 30 days. Two different reaction systems were applied to the experiments. One was for the reaction of the supercritical CO₂-water-mineral and the water was titrated at pH 8 (similar to brine water). The other was the reaction of supercritical CO₂-mineral without water.

Before the experiment, the mineral surface was observed by

using a reflecting microscope, and three locations on the surface were randomly selected for the image analysis of SPM (Digital Instrument, Multi Mode TM SPM) and then the average roughness value of those locations was analyzed to investigate the transmutation of mineral surface. ICP-OES (Perkin elmer, Optima 7000DV) analysis was conducted to measure the main compounds dissolved in solution of the high pressure cell and SEM/EDS (HITACHI, S-2400) analysis was done to identify the precipitants in high pressure cell after reaction.

Results for the experiment in the supercritical CO₂-water-plagioclase reaction showed that the average roughness value of the plagioclase surface was 0.155 nm before the experiment. It maintained for 20 days of the experiment, but considerably increased to 2.493 nm at 30 days. In case of the experiment of the supercritical CO₂-water-orthoclase reaction, the average roughness value of the surface was 0.372 nm before the reaction but it gradually increased to 1.141 nm until 20 days. For next 10 days, the average roughness value was considerably increased to 2.849 nm. Results of the supercritical CO₂-water-biotite reaction showed that the initial average roughness value was 0.659 nm, but gradually increased to 0.755 and 1.097 nm after 10 and 30 days, respectively. In the reaction without water, the average roughness values of all three mineral surfaces (plagioclase, orthoclase, and biotite) were almost identical for 30 days of the reaction, suggesting that the surface change of the mineral by supercritical CO₂ (without water) hardly occurred at CO₂ sequestration sites.

Variations of average roughness value of mineral surface were also observed by SPM images and it suggested that the dissolution and re-precipitation of minerals may occur by the reaction with the supercritical CO₂ and water in pore space of brine aquifer within several months. Results of the analysis of the solution in the cell at different reaction time intervals showed that the pH of the solution decreased to 4 as the supercritical CO₂ was dissolved. For the plagioclase, the concentrations of Ca²⁺ and Na⁺ in solution were 75 and 50 mg/L, respectively. For orthoclase, the concentrations of Al³⁺ and Ca²⁺ were higher than other ions and their concentrations were around 3 mg/L. For the biotite, concentrations of Na⁺ and K⁺ were 7 mg/L and 6 mg/L, respectively.

From SEM and EDS spectra analyses of the precipitant created in the high-pressurized cell, the precipitants were mostly composed of the amorphous silicate minerals including a large quantity of Ca²⁺. In case of the orthoclase, the precipitants in the cell consisted mainly of Al³⁺, Si⁴⁺ and O²⁻, which was very similar to a kaolinite. In case of the supercritical CO₂ and mineral reaction without water, the dissolution of mineral and the re-precipitation did not occur in the cell. It suggests that the phase change of mineral would be low in a supercritical CO₂-mineral reaction without water.

Key word : supercritical CO₂, underground sequestration, plagioclase, orthoclase, biotite, and average roughness value

Contents

Abstract	i
Contents	vi
List of Figures	
List of Tables	
 CHAPTER I. INTRODUCTION	 1
 CHAPTER II. OBJECTIVE	 4
 CHAPTER III. BACKGROUND	 5
3.1 Greenhouse effect	5
3.1.1 Carbon dioxide emission	6
3.2 Carbon dioxide capture and sequestration	8
3.3 CO ₂ sequestration mechanisms in geochemical formations	11
3.3.1 Stratigraphic and structural trapping	
3.3.2 Hydrodynamic and residual trapping	13
3.3.3 Solubility and mineral trapping	15
 CHAPTER IV. EXPERIMENTAL METHODS	 19
4.1 Mineral sample preparation for the experiments	19
4.1.1 Plagioclase	21
4.1.2 Orthoclase	23
4.1.3 Biotite	25

4.2	Reproduction of CO ₂ sequestration condition in lab scale	27
4.3	Dissolution and the surface change of minerals in the supercritical CO ₂ - water-mineral reaction	30
4.4	SEM and EDS Analyses on precipitants created from the supercritical CO ₂ -water-mineral reaction	33

CHAPTER V. RESULTS AND DISCUSSION

5.1	Results of the reproduction of CO ₂ sequestration condition in lab scale	36
5.2	Results of the dissolution and the surface change of minerals in supercritical CO ₂ -water- mineral reaction	
5.2.1	Plagioclase	39
5.2.2	Orthoclase	43
5.2.3	Biotite	47
5.2.4	Dissolution of plagioclase	52
5.2.5	Dissolution of orthoclase	53
5.2.6	Dissolution of biotite	54
5.3	Results of SEM/EDS analysis on precipitants created from supercritical CO ₂ -water-mineral reaction	
5.3.1	Precipitant created by the supercritical CO ₂ -water-plagioclase reaction	56
5.3.2	Precipitant created by the supercritical CO ₂ -water-orthoclase reaction	58

CHAPTER VI. CONCLUSIONS	61
-------------------------------	----

REFERENCES	65
ABSTRACT (KOREAN)	73
ACKNOWLEDGMENTS	
APPENDIX(PUBLICATIONS)	



List of Figures

Fig. 1. Schematic of the greenhouse effect on the earth surface (referred from United states Environmental Protection Agency (EPA), 1995)	6
Fig. 2. Various geochemical medium for CO ₂ sequestration (modified from Alberta geological survey)	10
Fig. 3. Photographs of stratigraphic and structural trapping, (a) fault trapping, (b) anticline or stratigraphic trapping, and (c) unconformity trapping) (referred from CO ₂ CRC (CO ₂ long-term future after injection))	12
Fig. 4. Schematic of CO ₂ injection into Utrira deep saline reservoir, Inset: location and extent of the Utsira formation (referred from Sleipner CO ₂ Storage Project)	14
Fig. 5. Storage security depends on a combination of physical and geochemical trapping (referred from ICPP, 2005)	17
Fig. 6. The single mineral samples ((a)plagioclase, (b)orthoclase, and (c)biotite) used in the experiments	20
Fig. 7. Photographs of (a)XRD and (b)XRF used in the experiment	20
Fig. 8. Result of XRD analysis for plagioclase	22
Fig. 9. Result of XRD analysis for orthoclase	24
Fig. 10. Result of XRD analysis for biotite	26
Fig. 11. Photographs of experimental equipments ((a)from the left, the cell in the water bath, back pressure regulator, and high pressure pump and (b)control software)	28

Fig. 12. Photographs of SPM (a) and ICP/OES (b) used in the experiments	31
Fig. 13. Schematic experimental system for supercritical CO ₂ -water-mineral reaction (referred from Choi et al, 2009b)	32
Fig. 14. Photographs of experimental devices ((a) high pressure cell, (b) control software and (c) the periodic high pressure pump and the back pressure regulator)	33
Fig. 15. Photographs of SEM (Scanning Electron Microscope, HITACHI (Japan) S-2400) coupled with EDS (Energy Dispersive X-Ray Spectrometer, KEVEX Ltd. SIGMA)	35
Fig. 16. Images for three phases of CO ₂ created in the high pressurized cell ((a) gas phase CO ₂ , (b) liquid phase CO ₂ , and (c) supercritical phase CO ₂)	37
Fig. 17. CO ₂ phases in the high pressurized cell plotted on the CO ₂ phase diagram at six different pressure and temperature conditions in Table 4 (referred from Span and Wagner, 1996)	38
Fig. 18. The plagioclase surface change visualized from SPM images at different reaction time for supercritical CO ₂ -water-plagioclase experiment ((a)before the experiment, (b)10 days, (c)20 days, and (d)30 days)	40
Fig. 19. The average roughness values on three locations of the plagioclase surface at different reaction time for supercritical CO ₂ - water-plagioclase experiment	41
Fig. 20. The plagioclase surface change visualized from SPM images	

at different reaction time for supercritical CO ₂ -plagioclase experiment ((a)before the experiment, (b)10 days, (c)20 days, and (d)30 days)	42
Fig. 21. The average roughness value on the location of the plagioclase surface at different reaction time for supercritical CO ₂ - plagioclase experiment (without water)	43
Fig. 22. The orthoclase surface change visualized from SPM images at different reaction time for the supercritical CO ₂ -water-orthoclase experiment ((a)before the experiment, (b)10 days, (c)20 days, and (d)30 days)	44
Fig. 23. The average roughness values at three locations of the orthoclase surface at different reaction time for supercritical CO ₂ -water-orthoclase experiment	45
Fig. 24. The orthoclase surface change visualized from SPM images at different reaction time for supercritical CO ₂ -orthoclase experiment ((a)before the experiment, (b)10 days, (c)20 days, and (d)30 days)	46
Fig. 25. The average roughness value on the location of the orthoclase surface at different reaction time for supercritical CO ₂ -orthoclase experiment (without water)	47
Fig. 26. The biotite surface change visualized from SPM images at different reaction time for the supercritical CO ₂ -water-biotite experiment ((a)before the experiment, (b)10 days,	

(c)20 days, and (d)30 days)	48
Fig. 27. The average roughness value on two locations of the biotite surface at different reaction time for supercritical CO ₂ -water-biotite experiment	49
Fig. 28. The biotite surface change visualized from SPM images at different reaction time for the supercritical CO ₂ -biotite experiment ((a)before the experiment, (b)10 days, (c)20 days, and (d)30 days)	50
Fig. 29. The average roughness value on the location of the biotite surface at different reaction time for supercritical CO ₂ -biotite experiment (without water)	51
Fig. 30. Result of the concentration of dissolved ions in the cell from supercritical CO ₂ -water-plagioclase reaction	53
Fig. 31. Result of the concentration of dissolved ions in the cell from supercritical CO ₂ -water-orthoclase reaction	54
Fig. 32. Result of the concentration of dissolved ions in the cell from supercritical CO ₂ -water-biotite reaction	55
Fig. 33. Images of the precipitant created from the supercritical CO ₂ -water- plagioclase reaction ((a) the photograph of a precipitant and (b) SEM image of the precipitant)	57
Fig. 34. Images of the precipitation created from the supercritical CO ₂ -water-orthoclase reaction ((a) the photograph of precipitants and (b) SEM image of the precipitants)	58

List of Tables

Table 1. Result of principle component analysis by XRF for plagioclase	22
Table 2. Result of principle component analysis by XRF for orthoclase	24
Table 3. Result of principle component analysis by XRF for biotite	26
Table 4. Temperature and pressure conditions applied in the cell for CO ₂ phase reproduction	29
Table 5. Result of the principle component analysis by EDS for the precipitant created from the supercritical CO ₂ -water-plagioclase reaction	57
Table 6. Result of the principle component analysis by EDS for the precipitant created from supercritical CO ₂ -water-orthoclase reaction	59

CHAPTER I . INTRODUCTION

UN Framework Convention on Climate Change (UNFCCC), which has been organized by 189 nations, insists that the world should achieve the atmospheric reduction of CO₂ emission to prevent 'dangerous anthropogenic interference with the climate system', although the tolerance limit of atmospheric CO₂ concentration has not yet been quantified (UNFCCC, 1992). Anthropogenic emissions of CO₂, mainly from the burn of fossil fuels, are increasing natural greenhouse gas effects. Carbon dioxide concentration in the atmosphere has rapidly increased from 280 ppm in pre-industrial times to 380 ppm recently (Houghton et al., 1997). If the mankind does not maintain CO₂ emissions to present-day levels, the global warming and the climate change will be irreversible by 2050 when CO₂ concentration in the atmosphere will reach 550 ppm (Ketzer et al., 2009).

There are many kinds of technical processes to reduce CO₂ emissions in the atmosphere and the geological sequestration is considered as one of the most available processes (Hitchen, 1996; Akimoto et al., 2004; Emberlry et al., 2004). Geological sequestration includes the capture, the transport and the storage of CO₂ in geological medium, which are consisting of the separation of CO₂ from industrial and energy-related sources, the transport to a storage location such as coal beds, petroleum fields and deep saline formations, and finally the permanent isolation from the atmosphere.

Specially the deep brine aquifer (deep underground porous reservoir rocks saturated with brine) can be used for the storage of CO₂ and its CO₂ storage capacity is likely to be at least 1000 GtCO₂(IPCC, 2005). CO₂ can remain trapped in the brine aquifer by virtue of a number of mechanisms, such as physical trapping in the pore spaces of the aquifer, dissolution in the aquifer fluid (brine), and mineralization reacting with minerals to produce carbonate or hydroxide minerals. For the safety of CO₂ sequestration, injected CO₂ should be stored for very long periods of time and become less mobile as results of multiple trapping mechanisms. Research to predict what happens when CO₂ is injected into the brine aquifer is essential to decide the available aquifer for CO₂ sequestration in safe.

At most of CO₂ sequestration aquifer, CO₂ is captured below 800 m in depth, and gaseous CO₂ changes into the supercritical fluid phase because of high pressure and temperature. Many researchers agree that the supercritical CO₂ in the aquifer will affect on the minerals of rocks and thus change the hydrogeological properties of the original aquifer. The quantitative understanding for the dissolution and/or the secondary mineral precipitation derived from the supercritical CO₂-water-mineral reaction is necessary to calculate the true potential of the sequestration site, to decide the available brine aquifer as the CO₂ sequestration site and also to prevent the leaking accident of CO₂ from the storage site.

Geochemical reactions between minerals and water occurred at the subsurface (high temperature and pressure condition) have

been widely investigated from theoretical studies solving thermodynamic equations (Span and Wagner, 1996). However, the geochemical reactions in the supercritical CO₂-water-mineral have been rarely investigated by laboratory experiments. Dissolution and secondary precipitation of mineral caused by supercritical CO₂ at various time scales should be investigated in the subsurface condition. Sandstone formation have high porosity isolated impermeable layers is known to the most successful sequestration site and the coarse grained sandstone formation (Nakdong formation) of Kyungsang formation group in Korea is considered as the available site for CO₂ sequestration (referred from Kim, 2009). Feldspars and biotite are typical minerals having high reactivity in geochemical (Nesbitt and Young, 1984) and are also abundant minerals of Nakdong formation. Numerous studies revealed the dissolution mechanism of feldspars based on various surface reaction models (Helgeson et al., 1984) and the reaction rates for feldspars have been experimentally determined at different conditions (varying temperature, pressure, pH, and dissolved solution) (Sorai et al., 2007).

This study focused on the investigation for the dissolution and the secondary precipitation process of feldspars and biotite occurred from the supercritical CO₂-water-mineral geochemical reaction at CO₂ sequestration sites. Meaningful data and information about what happen in CO₂ sequestration site and how to control the geochemical reactions for the successful CO₂ storage will be derived from the experiments.

CHAPTER II. OBJECTIVE

Objective of this research is to investigate the geochemical reaction of minerals (plagioclase, orthoclase, and biotite) contacted with supercritical CO₂ in the CO₂ sequestration site.

This study is divided into three main experimental objectives;

- 1) To reproduce the CO₂ sequestration condition of the subsurface in the high pressurized cell.
- 2) To quantify the surface change and the dissolution of minerals contacted with supercritical CO₂ at CO₂ sequestration sites.
- 3) To investigate the main compounds and structures of precipitants produced in the supercritical CO₂-water-mineral reaction.

CHAPTER III. BACKGROUND

3.1 Greenhouse effect

The greenhouse effect is the phenomenon rising the temperature of the earth surface because specific gases such as water vapor, carbon dioxide, nitrous oxide, and methane in the atmosphere. These greenhouse gases in the atmosphere behave much like the glass panes in a greenhouse when sunlight enters the earth's atmosphere, passing through the blanket of greenhouse gases. As it arrives in the earth's surface, land, water, and biosphere absorb the sunlight's energy. Once absorbed, this energy is sent back into the atmosphere. Some of the energy passes back into space, but much of it remains trapped in the atmosphere by the greenhouse gases, causing the earth surface to heat up. Fig. 1 shows the schematic of the greenhouse effect occurred on the earth surface.

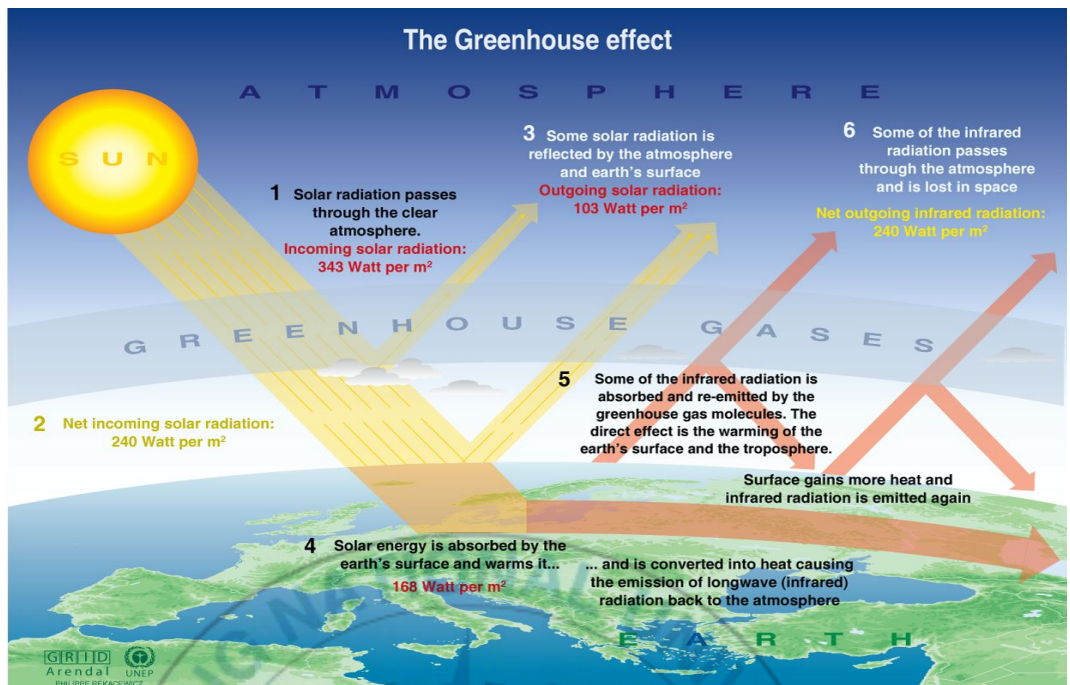


Fig. 1. Schematic of the greenhouse effect on the earth surface (referred from United states Environmental Protection Agency (USEPA), 1995).

3.1.1 Carbon dioxide emission

CO₂ emissions into the atmosphere has been considered as the most serious source to accelerate the greenhouse effect (Crowley, 2000). CO₂ emissions from various sources have been estimated by IEA (2003) and the power plant is the single largest source of CO₂ emissions. Other sources where CO₂ emissions arise from a few large point sources are other energy industries such as oil refineries, coal mining, oil/gas extraction, and the manufactory of

solid fuels. Emissions from the transport, the second largest source, have been growing faster than those from energy and industry in the last few decades (IPCC, 2001a); a key difference is that transport emissions are mainly from a multiplicity of small, distributed source.

The global radiative forcing of anthropogenic CO₂ is approximately 60 % of the total due to all anthropogenic greenhouse gases and the contribution from fossil fuel burn alone is about half of the total from all greenhouse gases (IPCC, 2001b). In terms of impact on radiative forcing, methane is the next most important anthropogenic greenhouse gas after CO₂ (IPCC, 2001b). The energy sector is an important source of methane but agriculture and domestic waste disposal contribute more the global total (IPCC, 2001c). Nitrous oxide contributes directly to climate change (current 6 % of the total impact of all greenhouse gases); the main source is agriculture but another is the industrial production of some chemicals (IPCC, 2001c).

3.2 Carbon dioxide capture and sequestration

Capturing CO₂ typically includes separating it from a gas stream and suitable capturing techniques were developed 60 years ago in connection with the production of town gas; there involved scrubbing the gas stream with a chemical solvent (Siddique, 1990). Then they were adapted to related purposes, such as capturing CO₂ from the chimney gas streams of coal or gas burning plant and enhancing oil recovery (EOR). These developments require improvements to the process so as to inhibit the oxidation of the solvent in the flue gas stream, which are widely used today for separating CO₂ and other acid gases from natural gas streams.

There are many processes available for the storage of CO₂. The first disposal of such a concept envisaged the injection of CO₂ into the ocean so that it was carried into deep water where, it was thought, it would remain for hundreds of year (Marchetti, 1977). In order to make a significant difference to the atmospheric loading of greenhouse gases, the amount of CO₂ that would need to be stored in this process would have to be significant compared to the amounts of CO₂ currently radiated to the atmosphere- in other words gigatonnes of CO₂ per year.

Other storage options have also been proposed. Injection of CO₂ underground would involve similar technology to that employed by the oil and gas industry for the exploration and production of hydrocarbons, and for the underground injection of waste as

practised in the USA. Wells would be drilled into geological formations and CO₂ would be injected. In some cases, this could lead to the enhanced production of hydrocarbons, which would help to offset the cost. An extension of this idea involves injection into saline formations (Koide et al., 1992) or into unminable coal seams (Gunter et al., 1997); in the latter case, such injection may sometimes result in the displacement of methane, which could be used as a fuel (Fig. 2).

Monitoring will be required both for purposes of managing the storage site and verifying the extent of CO₂ emissions reduction which has been achieved. Techniques such as seismic surveys, which have developed by the oil and gas industry, have been known to be adequate for observing CO₂ underground (Gale et al., 2001) and may form the basis for monitoring CO₂ stored in such reservoirs. Many alternatives to the storage of dense phase CO₂ have been proposed: for example, using the CO₂ to make chemicals or other products (Aresta, 1987), fixing it in mineral carbonates for storage in a solid form (Seifritz, 1990; Dunsmore, 1992), storing it as solid CO₂ ('dry ice') (Seifritz, 1992), as CO₂ hydrate, or as solid carbon (Steinberg, 1996).

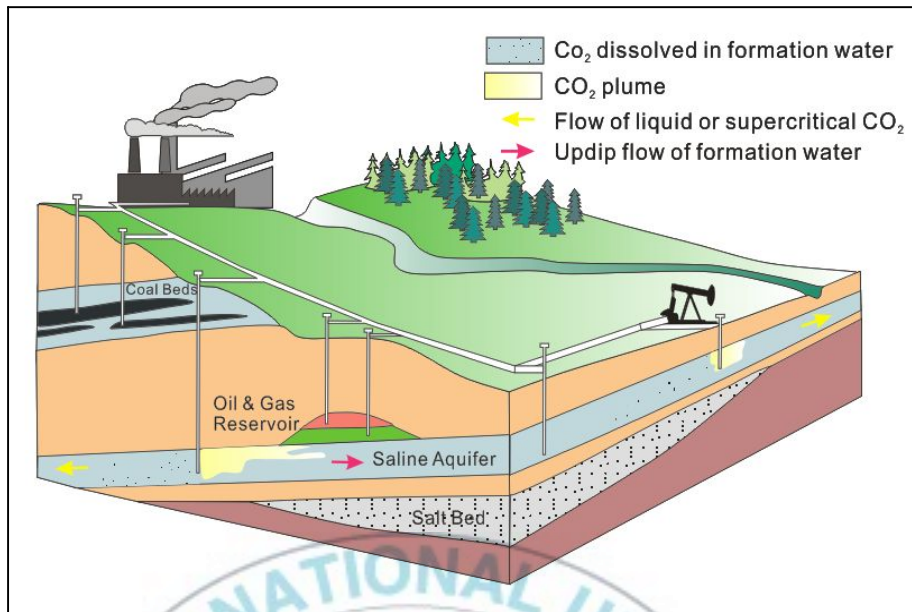


Fig. 2. Various geochemical medium for CO₂ sequestration (modified from Alberta geological survey, 2008).

3.3 CO₂ sequestration mechanisms in geological formations

The effectiveness of geological storage for CO₂ depends on a combination of physical (stratigraphic, structural and hydrodynamic) and geochemical (solubility and mineral) trapping mechanisms (Bachu et al., 2007). The most effective storage sites are those where carbon dioxide is permanently fixed because it is trapped under a thick, low-permeability cap rock or is transformed to solid minerals or is adsorbed on the surfaces of coal micropores (Bachu et al., 2007; IPCC, 2005).

3.3.1 Stratigraphic and structural trapping

Physical trapping of CO₂ below low-permeability seals (cap rocks), such as very-low-permeability shale or salt beds, is the important means to store CO₂ in geological formations (ICPP, 2005). In some high latitude areas, shallow gas hydrates may conceivably act as a seal. Sedimentary basins may have such closed, physically bound traps or structures, which are occupied mainly by saline water, oil, and gas. Structural traps include those formed by horizontal, folded or fractured rocks (Fig. 3. (b) and (c)). Faults can act as permeability barriers in some circumstances and as preferential pathways for fluid flow in other circumstances (Salvi et

al., 2000) (Fig. 3. (a)). Stratigraphic traps are formed by change in rock type caused by variation in the setting where the rocks were deposited. Both of these types of traps are suitable for CO₂ storage, although care must be taken not to exceed the allowable overpressure to avoid fracturing the cap rock or re-activating faults (Streit et al., 2005; IPCC, 2005).

The In Salah gas project, a joint venture among Sonatrach, BP, and Statoil located in the central Saharan region of Algeria, is the world's first large-scale CO₂ sequestration project in a gas reservoir (Riddiford et al., 2003). The Krechba Field at In Salah produces natural gas containing up to 10 % CO₂ from several geological reservoirs and delivers it to markets in Europe, after processing and stripping the CO₂ to meet commercial specifications.

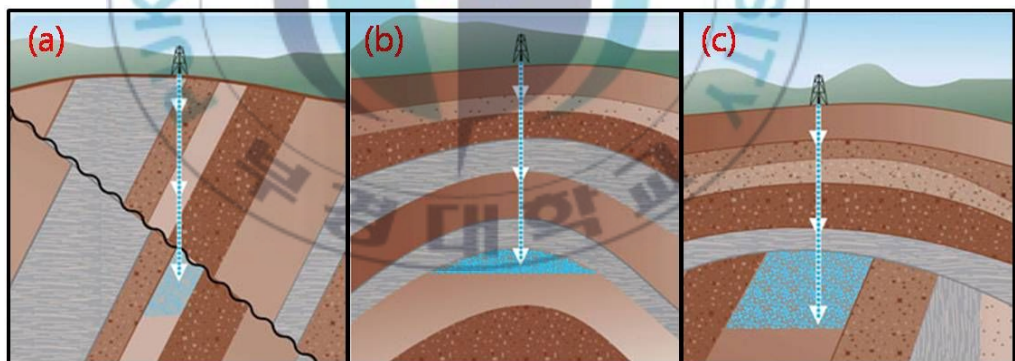


Fig. 3. Photographs of stratigraphic and structural trapping, (a) fault trapping, (b) anticline or stratigraphic trapping, and (c) unconformity trapping) (referred from CO₂CRC, 2008).

3.3.2 Hydrodynamic and residual trapping

Hydrodynamic trapping can occur in saline aquifer formations that do not have a closed trap, but where fluids migrate very slowly over long distances. When CO₂ is injected into a saline formation, it displaces saline water and then migrates buoyantly upwards, because it is less dense than the water. When it reaches the top of the formation, it continues to migrate as a separate phase until it is trapped as residual CO₂ saturation or in local structural or stratigraphic traps within the sealing formation. In the longer term, significant quantities of CO₂ dissolve in the saline formation water and then migrate with the groundwater. Where the distance from the deep injection site to the end of the overlying impermeable formation is hundreds or thousands of kilometers, the time scale for fluid to reach the surface from the deep basin can be millions of years (Bachu et al., 1994; IPCC, 2005).

The Sleipner Project, operated by Statoil in the North Sea about 250 km off the coast of Norway, is the first commercial scale project dedicated to geological CO₂ storage in a saline formation. The CO₂ (about 9 %) from Sleipner West Gas Field is separated, then injected into a large, deep, saline formation 800 m below the seabed of the North Sea. The Saline Aquifer CO₂ Storage (SACS) project was established to monitor and research the storage of CO₂ (ICPP, 2005) (Fig. 4).

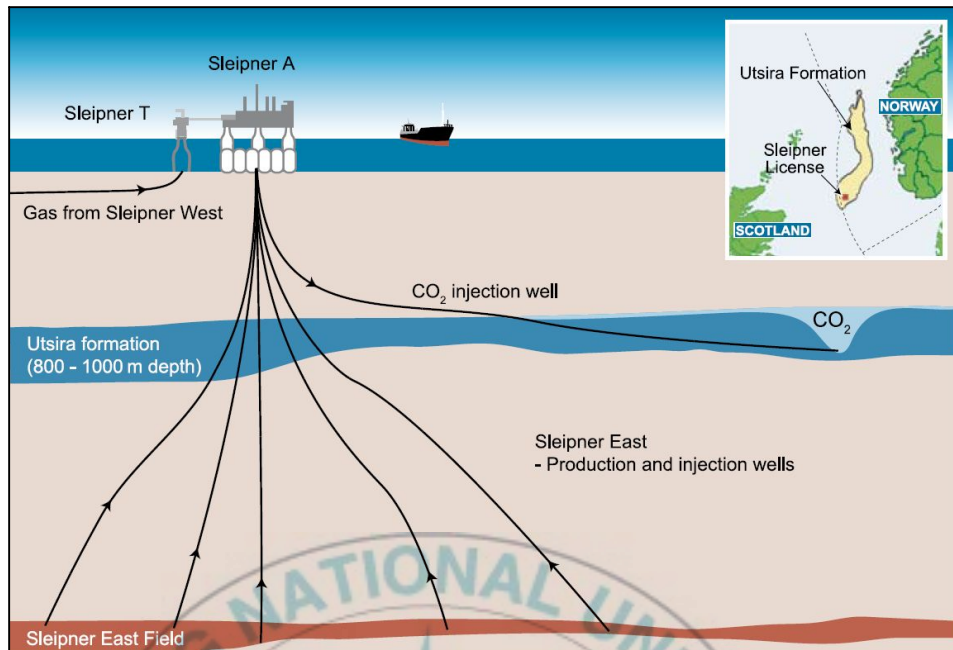


Fig. 4. Schematic of CO₂ injection into Utrira deep saline reservoir, Inset: location and extent of the Utsira formation (referred from Sleipner CO₂ Storage Project, 2004).

3.3.3 Solubility and mineral trapping

Carbon dioxide in the subsurface can undergo a sequence of geochemical interactions with the formation water and minerals of the rock that will further change its storage capacity and effectiveness. First, when CO₂ dissolved in formation water, a process commonly called "solubility trapping" occurs. The important benefit of solubility trapping is that once CO₂ is dissolved, it no longer exists as a separate phase, thereby eliminating the buoyant forces that drive it upwards. Next, it will form ionic species as the rock dissolves, accompanied by a rise in the pH. Finally, some fraction maybe transformed to stable carbonate minerals (mineral trapping), the most permanent status of geological storage (Gunter et al., 1993). Mineral trapping is believed to be relatively slow, possibly taking a thousand years or longer. Nevertheless, the permanence of mineral storage, combined with the potentially large storage capacity present in some geological settings, makes this a desirable feature of long-term storage.

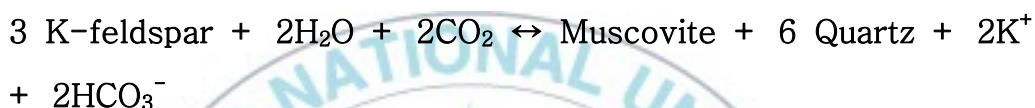
Dissolution of CO₂ in formation waters can be represented by the chemical reaction:



The CO₂ solubility in formation water decreases as temperature and salinity increase. Dissolution is fast when formation

water and CO₂ share the same pore space, but once the formation fluid is saturated with CO₂, the rate slows and is controlled by diffusion and convection rates.

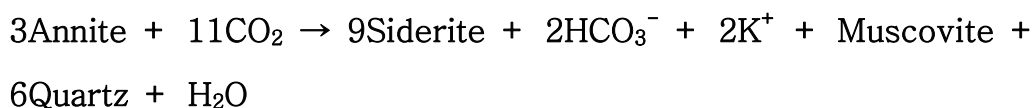
CO₂ dissolved in water makes a weak acid, which reacts with the sodium and potassium basic silicate or calcium, magnesium and iron carbonate or silicate minerals in the reservoir or formation to form bicarbonate ions by chemical reactions. The typical dissolution of K-feldspar with dissolved CO₂ is shown below;



From results of Choi's modeling for plagioclase, calcite and kaolinite will be precipitated by the supercritical CO₂-water-plagioclase reaction (Choi et al, 2009a) and the typical equation of plagioclase reaction with dissolved CO₂ and water is shown below;



In case of biotite, siderite, muscovite, and quartz will be precipitated by the supercritical CO₂-biotite reaction (Choi et al, 2009a). The typical dissolution of biotite with dissolved CO₂ is shown below;



Formation of carbonate minerals occurs from continued reaction of the bicarbonate ions with calcium, magnesium and iron from silicate minerals such as clays, micas, chlorites, and feldspars present in the rock matrix (Gunter et al., 1997; IPCC, 2005).

Fig. 5. shows that CO₂ sequester as almost the structural and stratigraphic trapping initially, but after time, the residual CO₂ trapping, the solubility trapping, and mineral trapping increase.

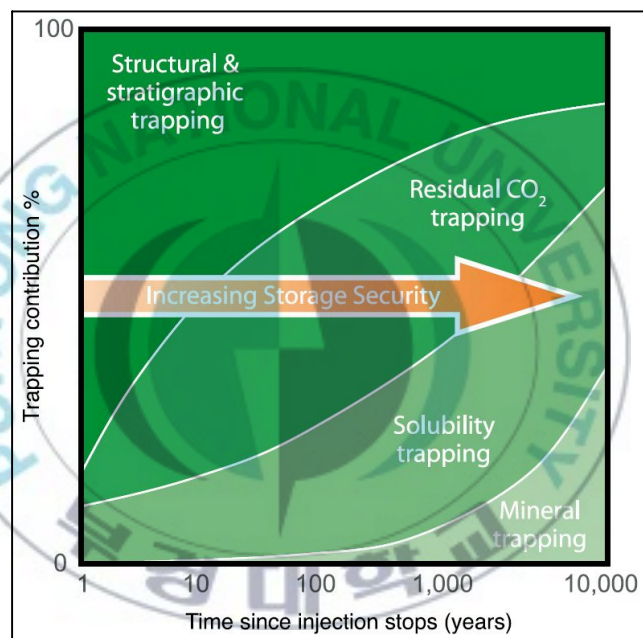


Fig. 5. Storage security depends on a combination of physical and geochemical trapping (referred from ICPP, 2005).

In this study, the dissolution of minerals and the secondary precipitation, occurred when minerals contact with supercritical CO₂ at the same temperature and pressure condition of CO₂ sequestration sites, will be reproduced in the laboratory. Results from the experiment will support lots of academic and technical information necessary to decide the available CO₂ sequestration aquifer.



CHAPTER IV. EXPERIMENTAL METHODS

4.1 Mineral sample preparation for the experiments

Three single mineral samples used in experiments were orthoclase, plagioclase and biotite, which were purchased from WARD's Natural Science (USA). The main components and structure of each mineral sample were investigated from the analysis on XRF (X-Ray Fluorescence Spectrometer, Shimadzu XRF-1700) and XRD (X-Ray Diffractometer, Philips X'Pert-MPD System) (Fig. 6). The surface of each mineral was polished by the sandpaper of #1000 and #2000, then it was finally polished using a DAP-V disk (Sturuers Inc.) with diamond paste (6, 3 and 1 μm) (Fig. 7). The polished single mineral was cut a few millimeters (10 mm \times 10 mm) with a diamond cutter for the experiments.



Fig. 6. Photographs of (a)XRD and (b)XRF used in the experiment.

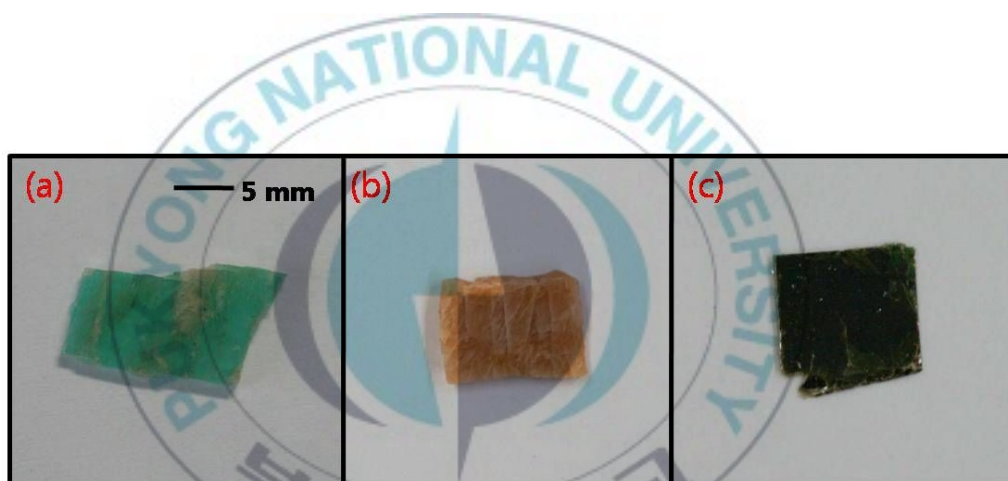


Fig. 7. The single mineral samples ((a)plagioclase, (b)orthoclase, and (c)biotite) used in the experiments.

4.1.1 Plagioclase

Plagioclase is a major constituent mineral in the Earth's crust, and is consequently used as an important diagnostic tool in petrology for identifying the composition, origin and evolution of igneous rocks. Plagioclase is an important series of tectosilicate minerals within the feldspar family. Rather than referring to a particular mineral with a specific chemical composition, plagioclase is a solid solution series, more properly known as "plagioclase feldspar series". The series ranges from albite to anorthite endmembers (with respective compositions from $\text{NaAlSi}_3\text{O}_8$ to $\text{CaAl}_2\text{Si}_2\text{O}_8$), where sodium and calcium atoms can substitute for each other in the mineral's crystal lattice structure (Rock-forming minerals). The plagioclase feldspar series includes the six minerals albite, oligoclase, andesine, labradorite, bytownite, and anorthite : the divisions are taken at anorthite mol. percentages 0-10, 10-30, 30-50, 50-70, 70-90 and 90-100, respectively.

The plagioclase sample for the experiment was the anorthite containing 20.59, 11.76 and 2.70 % of Al^{3+} , Ca^{2+} and Na^+ , respectively (Table 1) and Fig. 8 shows XRD peaks of the sample, which is similar to the typical anorthite XRD peaks.

Table 1. Result of principle component analysis by XRF for plagioclase

Material	Plagioclase	Plagioclase	Plagioclase	Plagioclase	S.D.
Name	(1/3)	(2/3)	(3/3)	(Average)	
SiO ₂	50.96	50.95	51.00	50.97	0.0748
Al ₂ O ₃	20.59	20.60	20.58	20.59	0.0287
TiO ₂	0.14	0.15	0.14	0.14	0.0038
Fe ₂ O ₃	6.96	6.97	6.97	6.97	0.1123
MnO	0.12	0.12	0.12	0.12	0.0064
MgO	5.40	5.44	5.42	5.42	0.0200
CaO	11.76	11.77	11.77	11.76	0.0627
Na ₂ O	2.71	2.70	2.68	2.70	0.0050
K ₂ O	0.34	0.34	0.34	0.34	0.0130
P ₂ O ₅	0.00	0.00	0.00	0.00	0.0015
LOI	0.57	0.57	0.57	0.57	
Total	99.55	99.61	99.59	99.58	

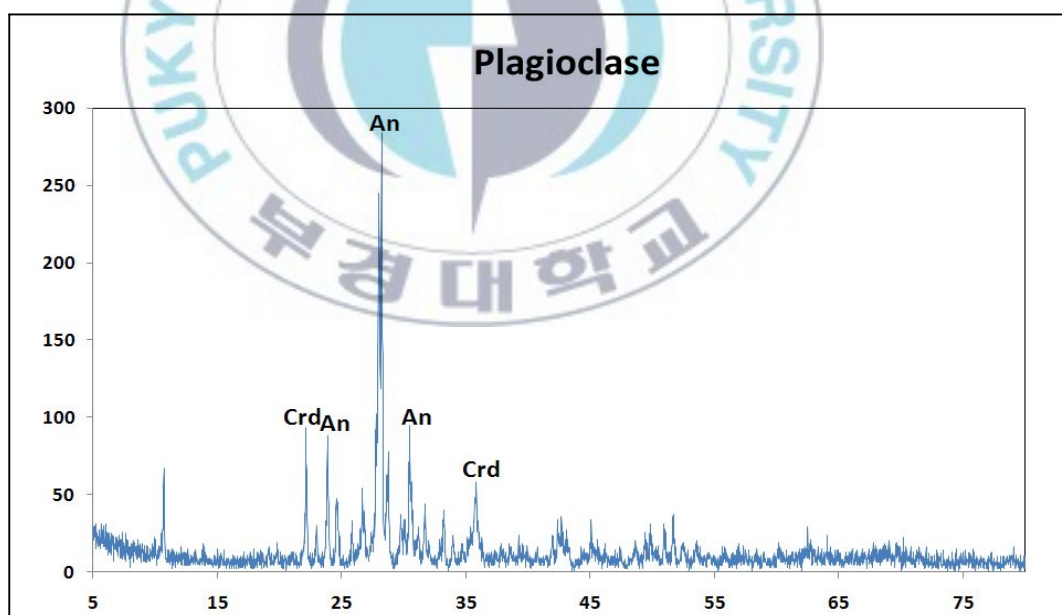


Fig. 8. Result of XRD analysis for plagioclase.

4.1.2 Orthoclase

Orthoclase is a common constituent of most granites and other felsic igneous rocks and often forms huge crystals and masses in pegmatite. Typically, the pure potassium endmember of orthoclase forms a solid solution with albite, the sodium endmember. The alkali feldspars are essentially a series varying from KAlSi_3O_8 to $\text{NaAlSi}_3\text{O}_8$ but normally also contain amount of $\text{CaAl}_2\text{Si}_2\text{O}_8$ in solid solution. Other ions, which maybe percent in limites amounts include Ba^{2+} , Ti^{3+} , Fe^{3+} , Fe^{2+} , Mg^{2+} , Sr^{2+} , and rarely Mn^{2+} . Result of XRF analysis for the orthoclase sample shows experiment, it was K-feldspar containing 16.20, 12.32, and 1.22 % of Al^{3+} , K^+ , and Na^+ , respectively (Table 2). XRD peaks of the sample equal to the typical orthoclase XRD peaks (Fig. 9).

Table 2. Result of principle component analysis by XRF for orthoclase

Material Name	Orthoclase (1/3)	Orthoclase (2/3)	Orthoclase (3/3)	Orthoclase (Average)	S.D.
SiO ₂	68.94	68.93	68.97	68.95	0.0488
Al ₂ O ₃	16.20	16.22	16.20	16.20	0.0227
TiO ₂	0.01	0.01	0.01	0.01	0.0020
Fe ₂ O ₃	0.00	0.09	0.00	0.00	0.0275
MnO	0.01	0.01	0.01	0.01	0.0042
MgO	0.01	0.00	0.00	0.01	0.0017
CaO	0.11	0.11	0.11	0.11	0.0077
Na ₂ O	1.24	1.20	1.22	1.22	0.0054
K ₂ O	12.32	12.32	12.32	12.32	0.0456
P ₂ O ₅	0.00	0.00	0.00	0.00	0.0042
LOI	0.58	0.58	0.58	0.58	
Total	99.42	99.48	99.43	99.41	

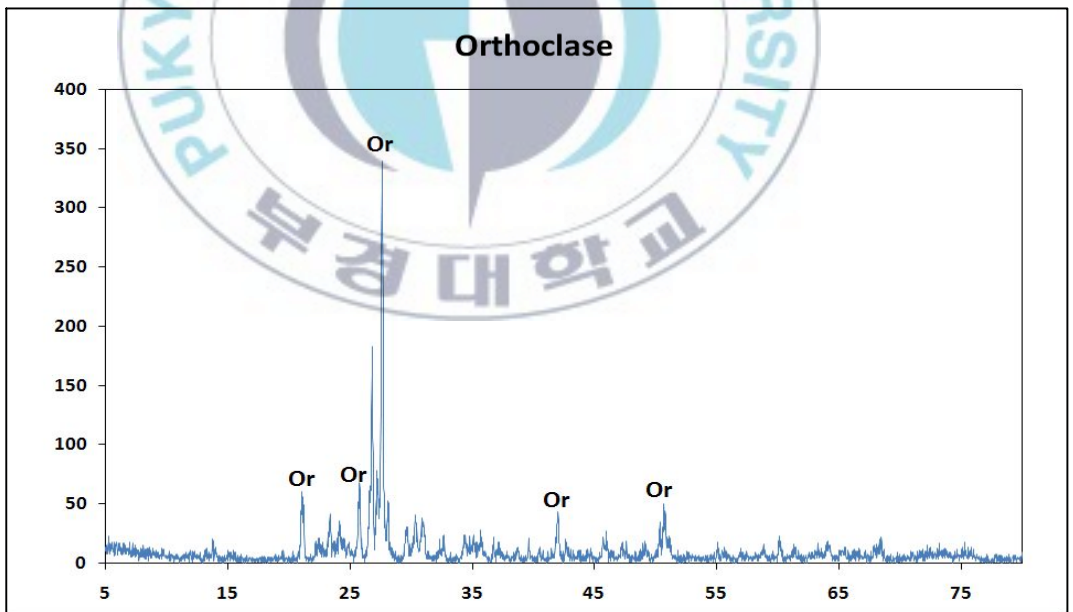


Fig. 9. Result of XRD analysis for orthoclase.

4.1.3 Biotite

The biotite is found in a wide variety of igneous and metamorphic rocks. Biotite is a common phyllosilicate mineral within the mica group, with the approximate chemical formula $K(Mg, Fe)_3AlSi_3O_{10}(F, OH)_2$. More generally, it refers to the dark mica series, primarily a solid-solution series between the iron-endmember annite, and the magnesium-endmember phlogopite. Iron, magnesium, aluminium, silicon, oxygen and hydrogen form sheets that are weakly bond together by potassium ions. Biotite has a highly perfect basal cleavage, and consists of flexible sheets, or lamellae, which easily flake off. It has a monoclinic crystal system, with tabular to prismatic crystals with an obvious pinacoid termination.

The biotite sample for the experiment consisted of Fe^{2+} , Mg^{2+} and Al^{3+} as 19.56, 13.94 and 10.84 %, respectively (Table 3) and Fig. 10 shows the XRD peaks of the biotite sample.

Table 3. Result of principle component analysis by XRF for biotite

Material Name	Biotite (1/3)	Biotite (2/3)	Biotite (3/3)	Biotite (Average)	S.D.
SiO ₂	40.41	40.46	40.45	40.44	0.0644
Al ₂ O ₃	10.83	10.84	10.83	10.84	0.0174
TiO ₂	2.19	2.20	2.19	2.20	0.0206
Fe ₂ O ₃	19.56	19.57	19.56	19.56	0.1645
MnO	0.62	0.63	0.62	0.63	0.0091
MgO	13.90	13.96	13.97	13.94	0.0298
CaO	0.22	0.22	0.22	0.22	0.0039
Na ₂ O	0.48	0.47	0.46	0.47	0.0035
K ₂ O	9.94	9.93	9.93	9.94	0.0726
P ₂ O ₅	0.01	0.01	0.01	0.01	0.0019
LOI	1.21	1.21	1.21	1.21	
Total	99.38	99.50	99.44	99.44	

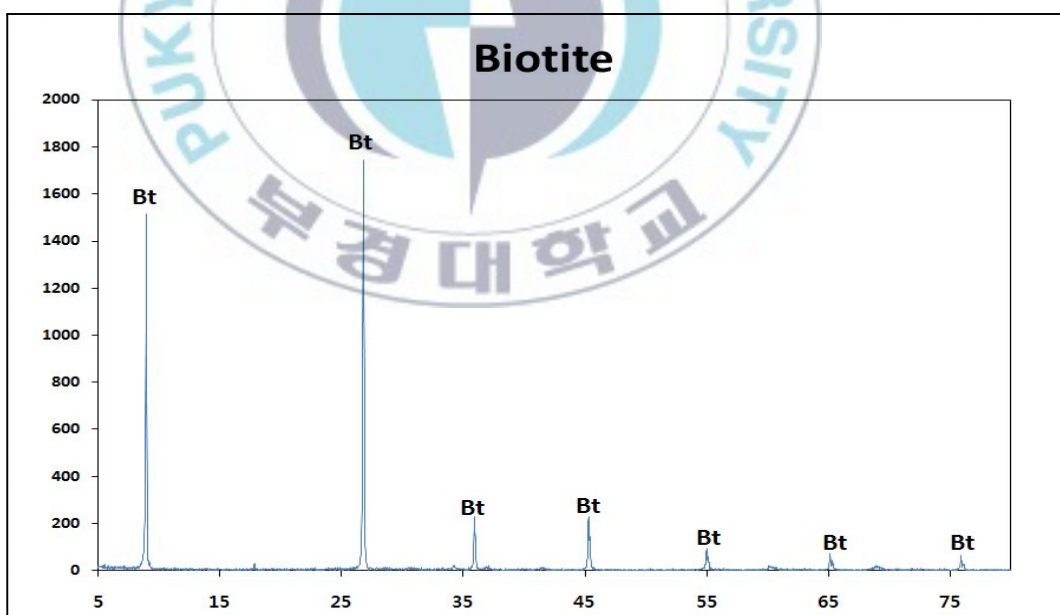


Fig. 10. Result of XRD analysis for biotite.

4.2 Reproduction of CO₂ sequestration condition in lab scale

For the experiment, it is necessary to verify if the supercritical CO₂ would be successfully created in the cell at the specific temperature and pressure condition. Laboratory scale experiments were performed to reproduce CO₂ sequestration conditions of the subsurface in the cell. The phase changes of CO₂ according to different temperature and pressure were investigated in the high pressurized cell and they were also compared to the theoretical results derived from the thermodynamic equations (Span et al., 1996; Vesovic et al., 1990). The cylinder shaped stainless steel cell (104 ml in capacity; purchased from Thar Inc.) having a transparent sapphire window (1 cm in diameter) was used to simulate the subsurface condition for CO₂ sequestration (Fig. 11. (a)). Six combinations of temperature and pressure, which were similar to the actual conditions of the subsurface, were applied to the cell and three different CO₂ phases (supercritical, liquid and gas phase) reproduced in the cell were visualized by using the high resolution camera (EOS 400D; purchased from Canon Inc.). Six temperature and pressure conditions for the experiment are in Table 4. The gaseous CO₂ (99.99 % of purity) was injected into the cell and the high pressure condition was applied inside of the cell by using the periodic high pressure pump and the back pressure regulator

(purchased from Thar Inc.). The cell was installed in the water bath to maintain the constant temperature during the experiment.

To get clear images for the phase change of CO_2 in the cell, 50 ml of distilled water was injected in to the cell and the inside of wall above the water surface of the cell was plastered with Sudan IV, which made organic solvents (containing "carbon") red. The CO_2 phase produced in the cell according to the specific temperature and pressure condition was visualized through the image window of the cell and their results were plotted in the CO_2 phase diagram, which was referred from Span and Wagner (1996).

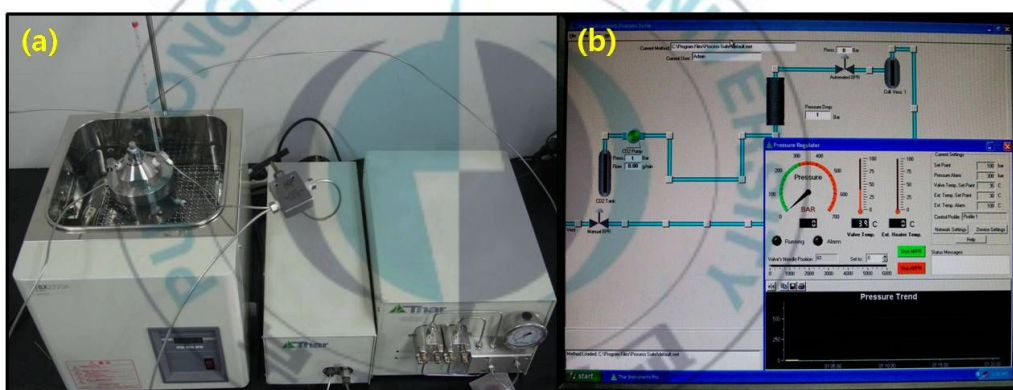
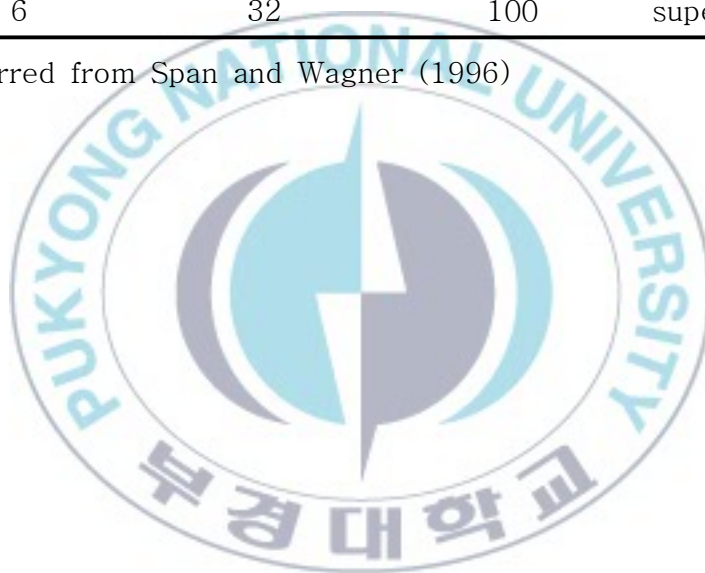


Fig. 11. Photographs of experimental equipments ((a)from the left, the cell in the water bath, back pressure regulator, and high pressure pump and (b)the software to control the experimental system).

Table 4. Temperature and pressure conditions applied in the cell for CO₂ phase reproduction

Condition No.	Temperature (°C)	Pressure (bar)	Theoretically calculated CO ₂ phase*
1	25	50	gas
2	25	80	liquid
3	35	60	gas
4	35	100	supercritical fluid
5	30	100	liquid
6	32	100	supercritical fluid

*: referred from Span and Wagner (1996)



4.3 Dissolution and the surface change of minerals in the supercritical CO₂- water-mineral reaction

Cleaved mineral samples detached from a fresh-single crystal were polished and cut a few millimeters (mostly 0.5 cm × 0.5 cm). After being washed with methanol, each mineral sample was glued on a 1.6 × 1.6 cm stainless steel plate. This plate was fixed on the sample holder in the high pressurized cell. To determine the dissolution characteristics of mineral from the measurement of surface change, it is necessary to compare the surface properties before and after the supercritical CO₂-water-mineral reaction and their surface images were analyzed on SPM (Scanning Probe Microscope). The mineral surface was observed using a reflecting microscope, and three locations on the surface were randomly selected for the observation with the SPM. Experiments for mineral dissolution and surface change were performed in two different conditions. First, a mineral reacted with supercritical CO₂ and distilled water (titrated pH 8 like seawater) in the cell because geosequestration sites as saline formations were deep sedimentary rocks saturated with formation waters or brines containing high concentrations of dissolved salts (IPCC, 2005). For the next experiment, the mineral samples were exposed to only supercritical CO₂ without water. For both experiments, the inside of the high-pressure cell was maintained at 100 bars and 50 °C for 30

days, the surface of each sample was observed using an SPM and the average roughness value of the sample surface was also measured by SPM every 10, 20 and 30 days in the experiment. The area of $20\ \mu\text{m} \times 20\ \mu\text{m}$ on three selected locations of the surface for each mineral sample was used for SPM analysis. In the case of the supercritical CO_2 -water-mineral experiment, water reacted with mineral and supercritical CO_2 was sampled from the cell at different time intervals and the main compounds (Ca^{2+} , Na^+ , K^+ , Al^{3+} , and Si^{4+}) dissolved in water were analyzed on ICP/OES (Perkin elmer, Optima 7000DV). Fig. 12 shows the photograph of SPM and ICP/OES used in the experiments.

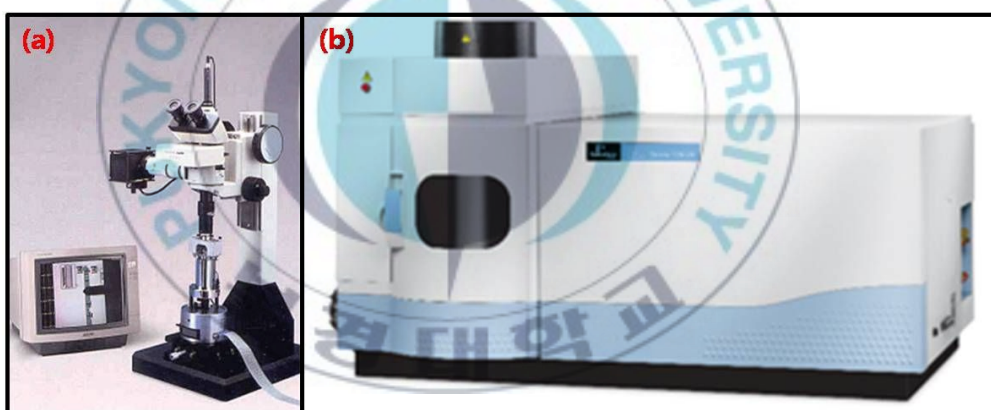


Fig. 12. Photographs of (a)SPM and (b)ICP/OES.

Batch experiments were performed at the supercritical CO_2 -water-mineral reaction system reproduced the high pressurized cell. The system consisted of a stainless steel cell (in capacity 104 ml), a injection tank, a CO_2 delivery pump (Thar, P-50), a back

pressure regulator (Thar, Automated BPR) and a control software (Thar, Thar instrument control software). The cell was located in an air-circulating oven (Sammi Inc., SM-520) to maintain thermostatically a constant temperature (50 °C). The half of the cell was filled with distilled water (pH 8) and the mineral sample was fixed on the holder attached in the cell. The gaseous CO₂ was injected into the cell from the CO₂ injection tank. The cell was highly pressurized by the periodic high pressure pump and the back pressure regulator (80 bar). Fig. 13 shows the schematic experimental system and Fig. 14 shows the photographs of experimental devices.

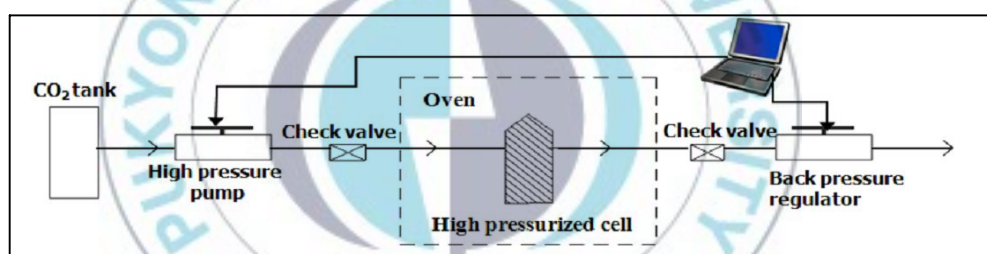


Fig. 13. Schematic experimental system for the supercritical CO₂-water- mineral reaction (referred from Choi et al, 2009b).

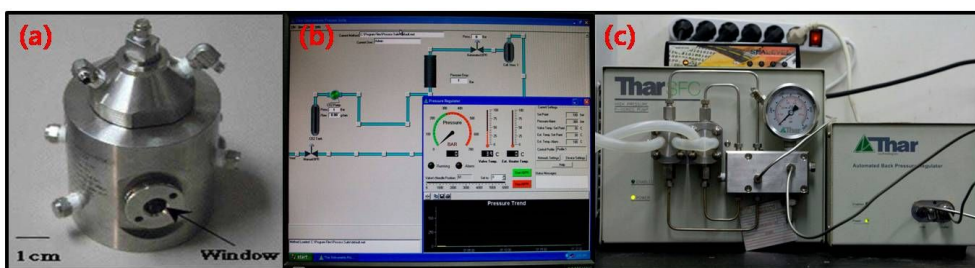


Fig. 14. Photographs of experimental devices ((a) the high pressure cell, (b) the control software and (c) the periodic high pressure pump and the back pressure regulator).



4.4 SEM and EDS Analyses on precipitants created from the supercritical CO₂-water-mineral reaction

SEM (Scanning Electron Microscope, model: HITACHI S-2400) and EDS (Energy Dispersive X-Ray Spectrometer, model: KEVEX Ltd. SIGMA) analyses were conducted to evaluate the structure and the main compositions of precipitants produced from the supercritical CO₂-water-mineral reactions. SEM is one of the useful equipments for visualizing the surface of the precipitation and EDS is also a useful instrument for evaluating the compositional characteristics of the material. For the analysis, precipitants in the cell were oven dried and mounted on a stainless steel slab with double-sided tape, followed by a coating of a thin layer of gold under vacuum to increase the electron conduction and to improve the quality of the micrographs. The acceleration voltage was constant at 20 kV and the microprobe was focused on the precipitation sample at a magnification of 4000. Fig. 15 shows the photographs of SEM and EDS used in the experiments.



Fig. 15. Photographs of SEM coupled with EDS used in the experiments.



CHAPTER V. RESULTS AND DISCUSSION

5.1 Results of the reproduction of CO₂ sequestration condition in lab scale

The images of CO₂ phases obtained from the window of the high pressurized cell showed the distinct differences among the gaseous CO₂, the liquid CO₂, and the supercritical CO₂ (Fig. 16). For the gaseous carbon dioxide, there was a colorless gas phase showing a distinct boundary with the distilled water underneath (Fig.16 (a)). For the phase of liquid carbon dioxide, the liquid carbon dioxide dyed red by Sudan IV was located at the middle of the distilled water underneath and the upper zero air (Fig. 16 (b)). In case of the supercritical fluid phase, CO₂ fluid had a orange color distinguished from the liquid phase and the gaseous phase and it moved freely in the cell (Fig. 16 (c)). Through this experiment, the gaseous carbon dioxide was observed in the cell at conditions 1 and 3 of Table 4 (under 73 bars). In condition of 2 and 5 in Table 4 with the temperature under 31.1 °C, the carbon dioxide existed as liquid in the cell. Finally, in the conditions 4 and 6 (the temperature over 31.1 °C and the pressure over 73 bars), the carbon dioxide in the cell existed as the supercritical fluid state. The video clip of images showed that the supercritical carbon dioxide moves significantly faster than the liquid carbon dioxide.

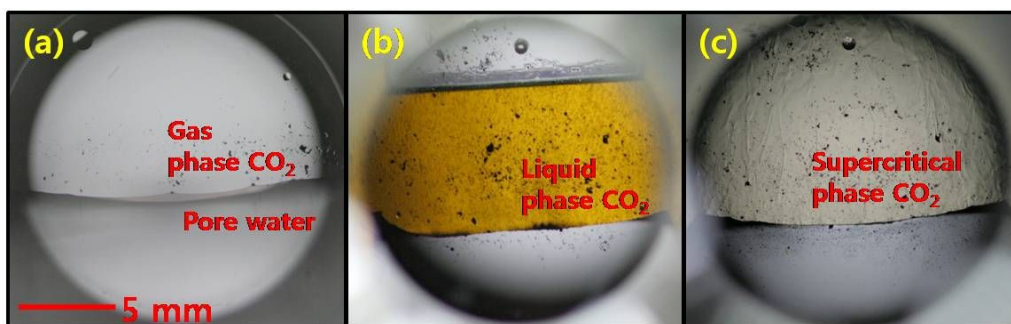


Fig. 16. Images for three phases of CO₂ created in the high pressurized cell ((a)gas phase CO₂, (b)liquid phase CO₂, and (c)supercritical phase CO₂).

CO₂ phases created in the cell at six temperature and pressure conditions were plotted on the CO₂ phase diagram referred from the theoretical thermodynamic equations to verify the successful reproduction of CO₂ phase in the experiment (Fig. 17). The experimental results for CO₂ phases in the cell matched with those from theoretical calculation, suggesting that the high pressurized cell system is available to simulate the geochemical reactions occurred in the subsurface for CO₂ sequestration.

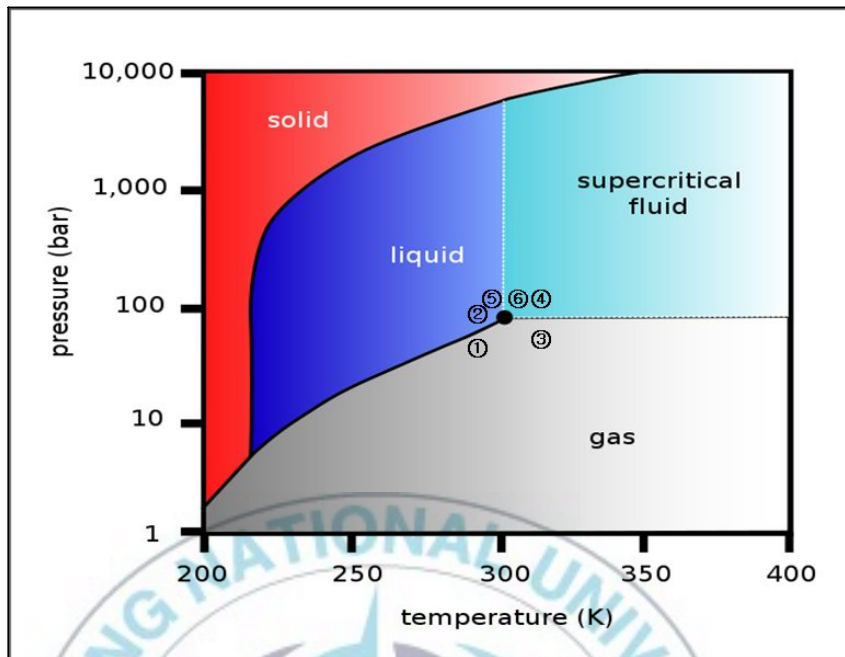


Fig. 17. CO₂ phases in the high pressurized cell plotted on the CO₂ phase diagram at six different pressure and temperature conditions in Table 4 (referred from Span and Wagner, 1996).

5.2 Results of the dissolution and the surface change of minerals in supercritical CO₂-water-mineral reaction

5.2.1 Plagioclase

Fig. 18. shows SPM images of an plagioclase mineral surface before and after the supercritical CO₂-water-plagioclase reaction. The surface of a plagioclase sample contacted with supercritical CO₂ and water was roughly changed with in 30 days of experiment, suggesting that the dissolution of minerals occurred in the cell at the subsurface condition (Fig. 18 (d)). The average roughness value of the plagioclase surface was 0.155 nm before the reaction, and then dramatically increased to 2.0 nm over 30 days of the reaction, showing 19 times increase of roughness values (Fig. 19). This result indicates that the plagioclase could be seriously weathered within several months when it comes into contact with the supercritical CO₂ and water at CO₂ sequestration site.

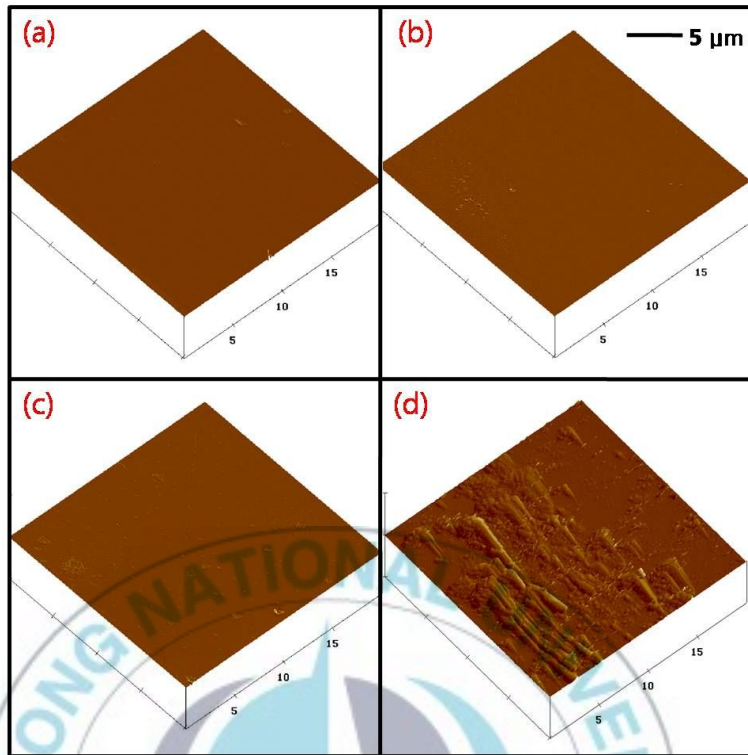


Fig. 18. The plagioclase surface change visualized from SPM images at different reaction time for supercritical CO₂-water-plagioclase experiment ((a)before the experiment, (b)10 days, (c)20 days, and (d)30 days).

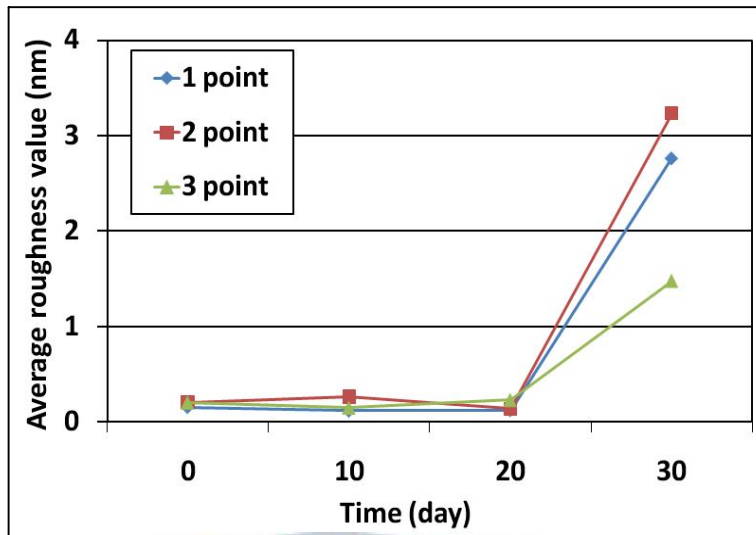


Fig. 19. The average roughness values on three locations of the plagioclase surface at different reaction time for supercritical CO₂-water-plagioclase experiment.

In the supercritical CO₂-plagioclase reaction (without water), SPM surface images showed that the plagioclase surface was not significantly changed and the mineral weathering did not occur by only supercritical CO₂ (Fig. 20). From SPM analysis, the average roughness value of the plagioclase surface decreased slightly from 0.345 nm to 0.172 nm over 10 days and maintain about 0.285 nm for the next 20 days (Fig. 21). It was suggested that plagioclase weathering would be low under supercritical CO₂-plagioclase reaction without water.

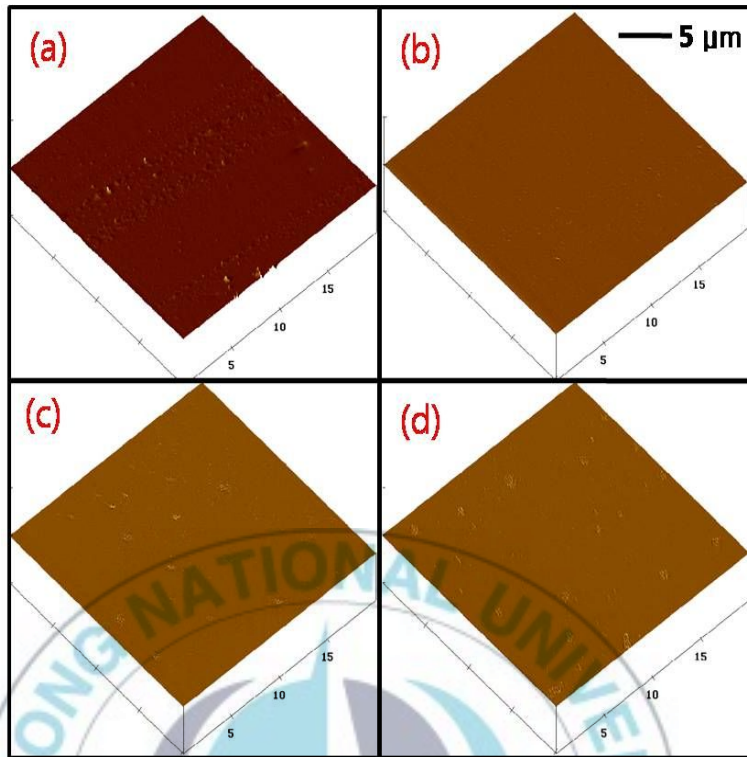


Fig. 20. The plagioclase surface change visualized from SPM images at different reaction time for supercritical CO₂-plagioclase experiment ((a)before the experiment, (b)10 days, (c)20 days, and (d)30 days).

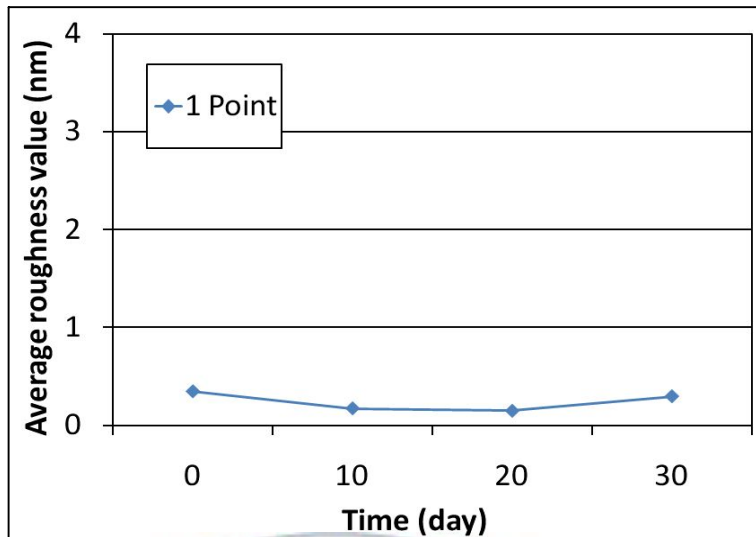


Fig. 21. The average roughness value on the location of the plagioclase surface at different reaction time for supercritical CO₂-plagioclase experiment (without water).

5.2.2 Orthoclase

Fig. 22 shows SPM images of a orthoclase crystal surface for 0-30 days under supercritical CO₂-water-orthoclase reaction. The surface was roughly changed by the dissolution for 30 days under the experiment. From the SPM analysis, the mineral average roughness value of three points on the mineral surface was 0.372 nm and it gradually increased to 1.141 nm after 20 days of the reaction (Fig. 23). For the next 10 days, the average roughness increased dramatically to 2.849 nm (about 8 times increase). This result also verifies that the orthoclase could be seriously weathered within several months when it comes into contact with the supercritical CO₂

and water.

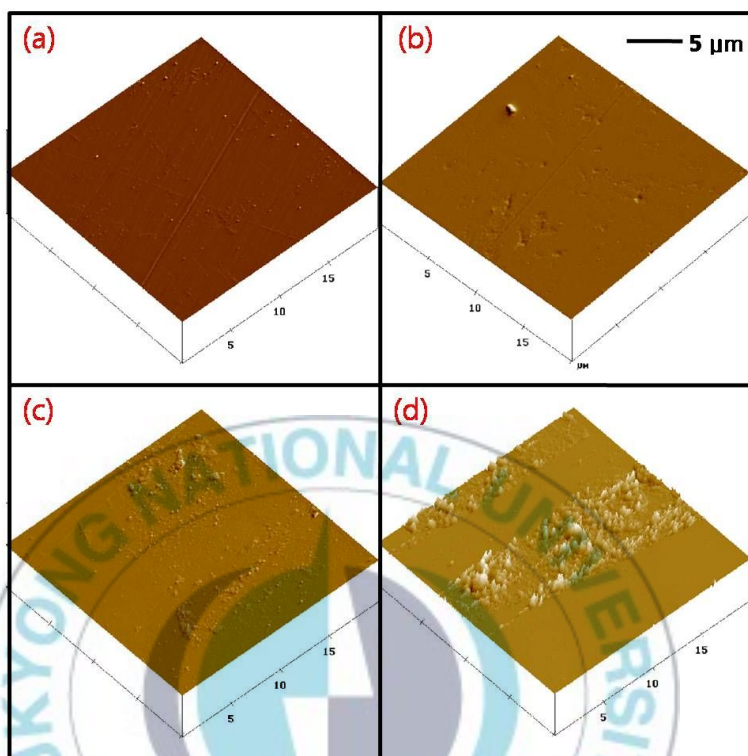


Fig. 22. The orthoclase surface change visualized from SPM images at different reaction time for the supercritical CO₂-water-orthoclase experiment ((a)before the experiment, (b)10 days, (c)20 days, and (d)30 days).

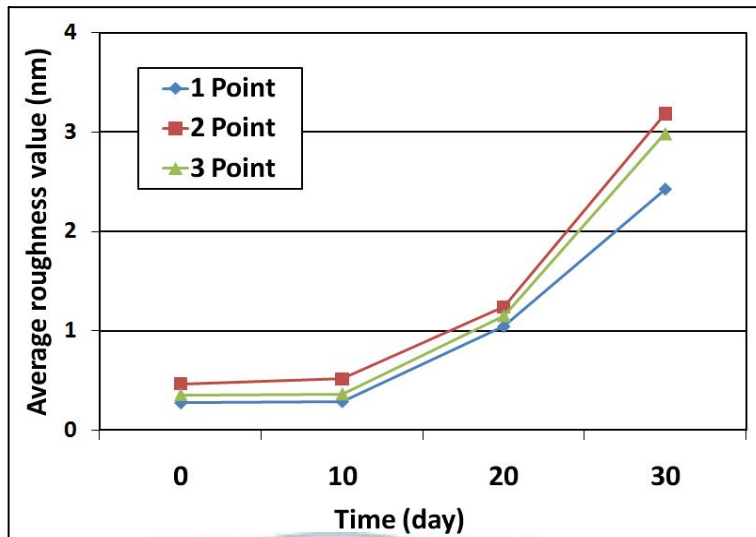


Fig. 23. The average roughness values at three locations of the orthoclase surface at different reaction time for supercritical CO₂-water-orthoclase experiment.

In the supercritical CO₂-orthoclase experiment, the surface of orthoclase was not significantly changed by supercritical CO₂ without water (Fig. 24). The initial average roughness value was 0.741 nm and it changed very little to 0.689 nm for 30 days of the experiment, suggesting that the weathering of orthoclase contacted with only supercritical CO₂ would be very low at CO₂ sequestration sites (Fig. 25).

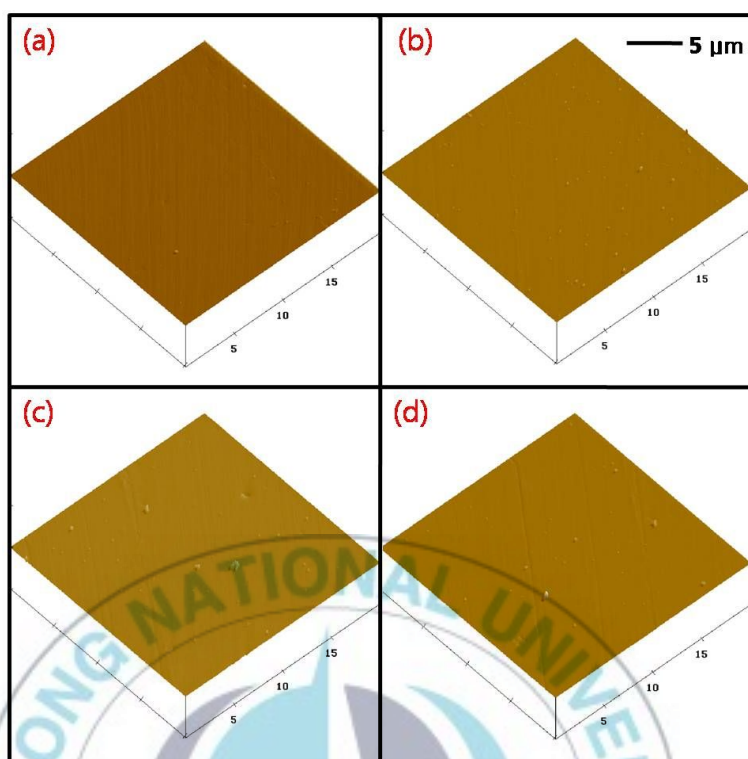


Fig. 24. The orthoclase surface change visualized from SPM images at different reaction time for supercritical CO₂-orthoclase experiment ((a)before the experiment, (b)10 days, (c)20 days, and (d)30 days).

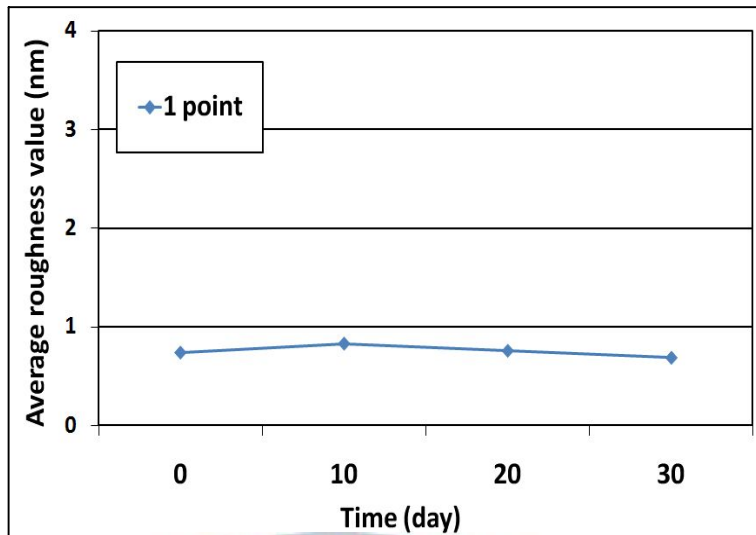


Fig. 25. The average roughness value on the location of the orthoclase surface at different reaction time for supercritical CO₂-orthoclase experiment (without water).

5.2.3 Biotite

Fig. 26 shows the SPM images of a biotite crystal surface for 0–30 days under the supercritical CO₂-water-biotite experiment. The biotite surface was changed by the dissolution for 30 days of the experiment. The initial average roughness value was 0.659 nm, and it gradually increased to 1.097 nm after 30 days (Fig. 27). This result indicates that the biotite could be weathered when it comes into contact with the supercritical CO₂ and water despite less than orthoclase and plagioclase.

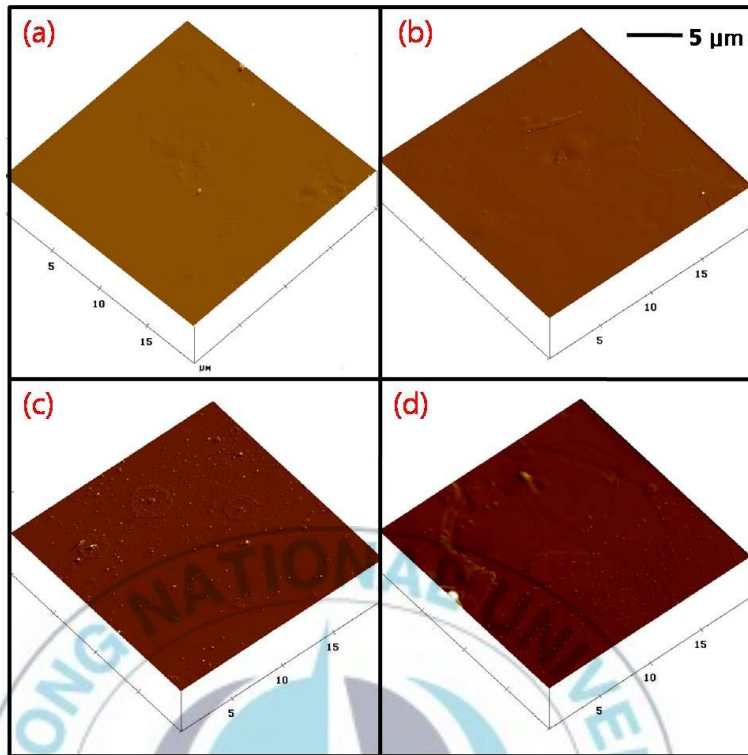


Fig. 26. The biotite surface change visualized from SPM images at different reaction time for the supercritical CO_2 -water-biotite experiment ((a)before the experiment, (b)10 days, (c)20 days, and (d)30 days).

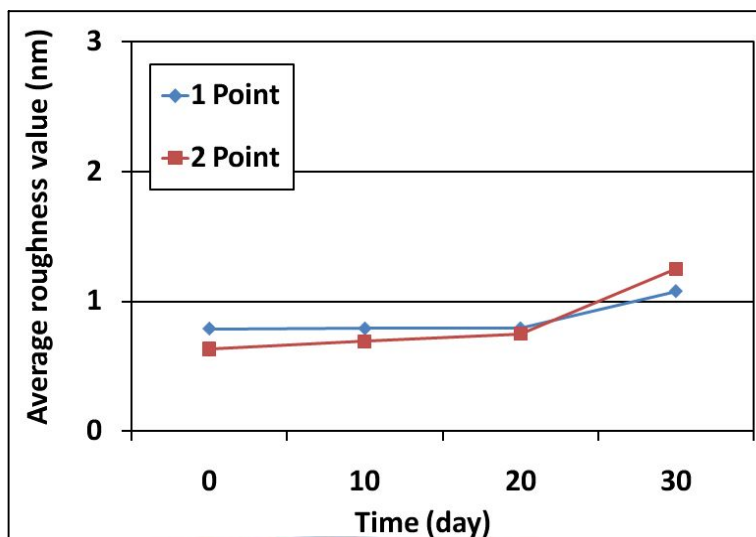


Fig. 27. The average roughness value on two locations of the biotite surface at different reaction time for supercritical CO₂-water-biotite experiment.

In the supercritical CO₂-biotite reaction without water, SPM surface images showed that the biotite surface was not significantly changed and the mineral weathering did not occur by only supercritical CO₂ (Fig. 28). The initial average roughness value was 0.481 nm and it changed very little to 0.401 nm for 30 days of the experiment, suggesting that the weathering of biotite contacted with only supercritical CO₂ would be low at CO₂ sequestration sites (Fig. 29).

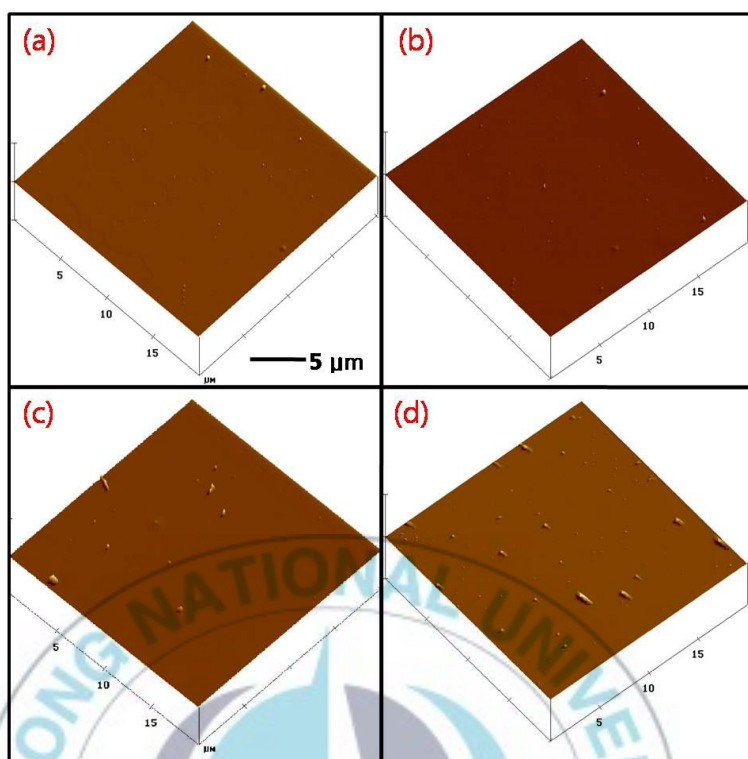


Fig. 28. The biotite surface change visualized from SPM images at different reaction time for the supercritical CO₂-biotite experiment ((a)before the experiment, (b)10 days, (c)20 days, and (d)30 days).

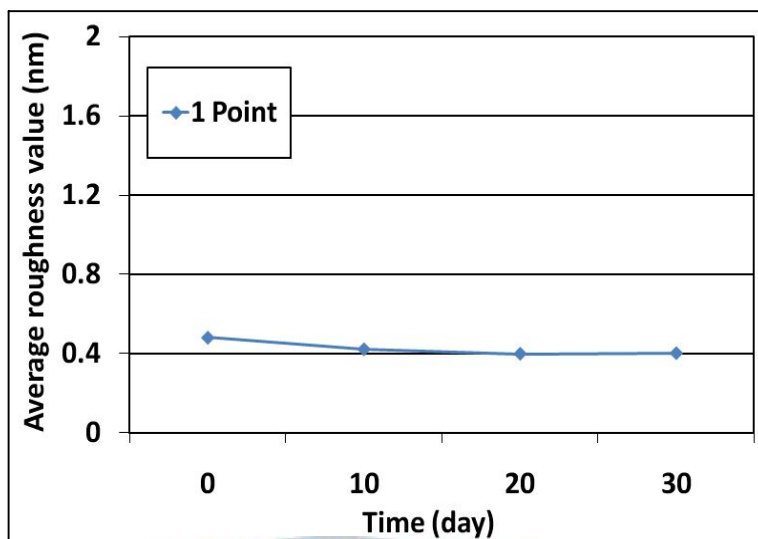
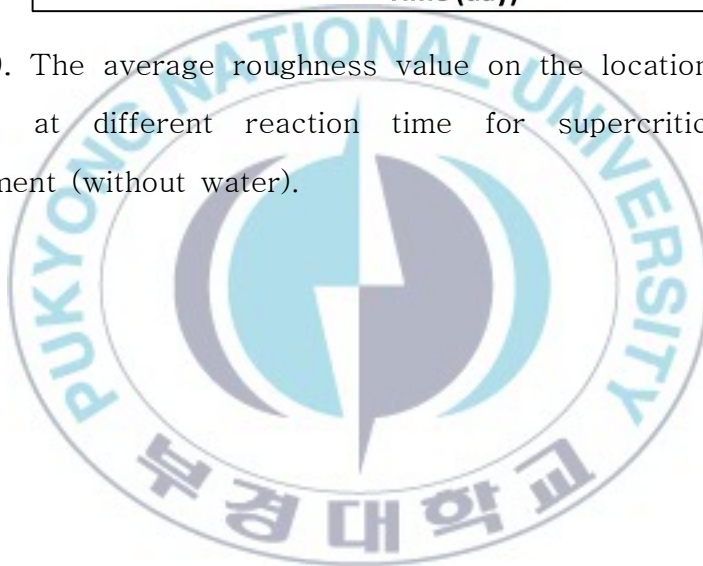


Fig. 29. The average roughness value on the location of the biotite surface at different reaction time for supercritical CO₂-biotite experiment (without water).



Five ml of water was sampled from the cell and the concentrations of cations dissolved from the mineral by the supercritical CO₂-water-mineral reaction. The pH change water in the cell was also measured by pH meter (Istek, EST-901M). The cations for ICP-OES analysis included Ca²⁺, Na⁺, K⁺, Al³⁺, Si⁴⁺, and Mg²⁺, which were main elements organizing rocks in the earth crust.

5.2.4 Dissolution of plagioclase

The pH of water decreased from 8 to 4 within 10 days as the supercritical CO₂ was dissolved in the water and it maintained around pH 4 for the whole experiment (Fig. 30). The dissolution of Ca²⁺ from the plagioclase linearly increased with the increase of the reaction time and Ca²⁺ concentration was 75 mg/L (Fig. 30). The dissolution of Na⁺ occurred a little for 20 days and dramatically increased for the next 10 days of the experiment. The final Na⁺ concentration in the water was 50 mg/L. These results suggested that Ca²⁺-rich plagioclase would be significantly dissolved when it contact with the supercritical CO₂ and water at CO₂ sequestration sites.

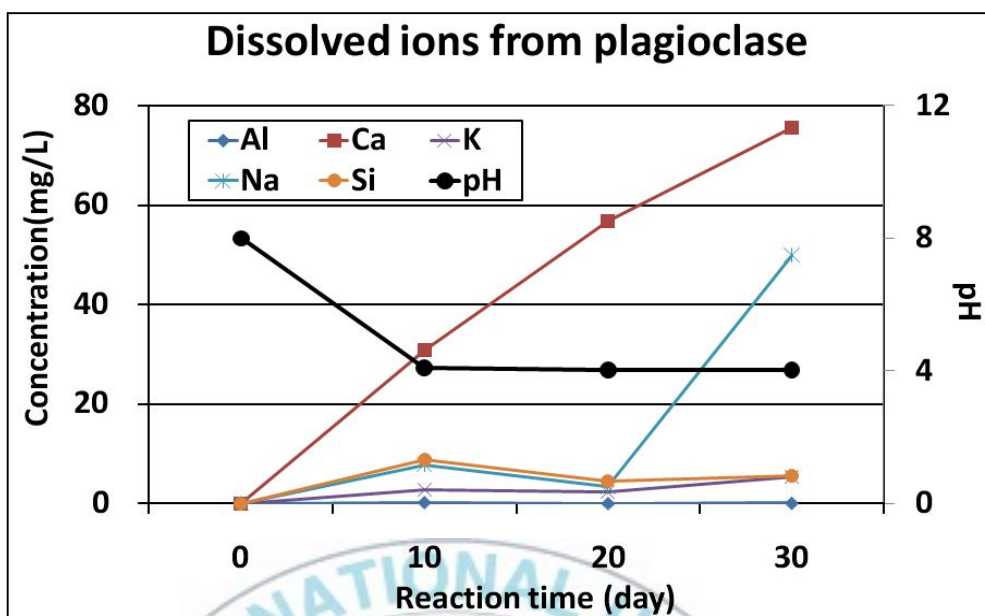


Fig. 30. Result of the concentration of dissolved ions in the cell from supercritical CO₂-water-plagioclase reaction.

5.2.5. Dissolution of orthoclase

Results of dissolution of analysis for water in the supercritical CO₂-water-plagioclase reaction were shown in Fig. 31. The pH of water decreased to pH 4, which was very similar to that in the plagioclase experiment. Even the orthoclase included high K⁺ content, Al³⁺, Ca²⁺, and Na⁺ were dissolved in order of their concentration, which were lower than 3 mg/L (Fig. 31). The concentrations of K⁺ and Si⁴⁺ were lower than 0.5 mg/L, suggesting that the dissolution of orthoclase would be dependant Ca²⁺ and Na⁺ rather than K⁺.

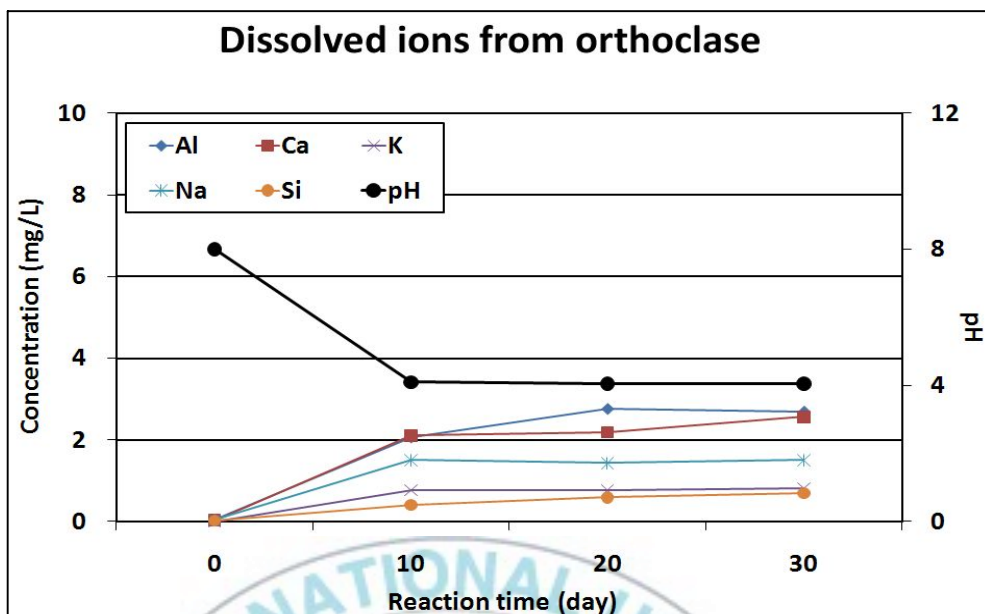


Fig. 31. Result of the concentration of dissolved ions in the cell from supercritical CO₂-water-orthoclase reaction.

5.2.6 Dissolution of biotite

For a biotite, the pH of water dropped to 4 by supercritical CO₂ dissolution after 10 days like other mineral dissolutions. Na⁺, K⁺, Ca²⁺, Al³⁺, Si⁴⁺, and Mg²⁺ were dissolved from the biotite in order of their concentration and the concentration of Na⁺, K⁺, and Ca²⁺ higher than 5 mg/L (Fig. 32). These results suggested that the main elements dissolved from the biotite were not Mg²⁺, Si⁴⁺, and Al³⁺ but Na⁺, K⁺, and Ca²⁺ when it contacted with the supercritical CO₂ and water at CO₂ sequestration sites.

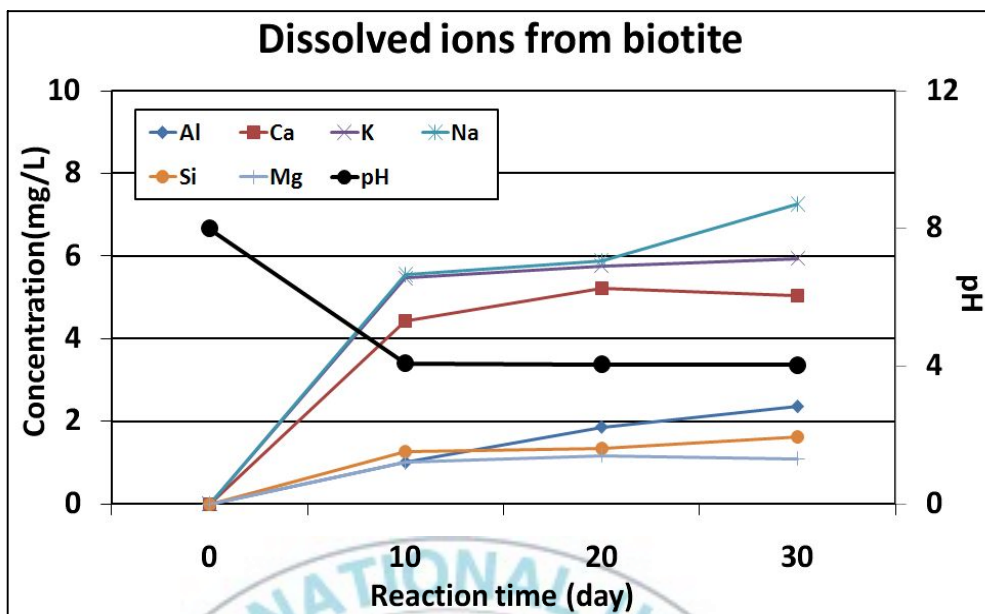


Fig. 32. Result of the concentration of dissolved ions in the cell from supercritical CO₂-water-biotite reaction.

5.3 Results of SEM/EDS analysis on precipitants created from supercritical CO₂-water-mineral reaction

The precipitation from dissolved ions in the high-pressure cell occurred because of the supercritical CO₂-water-feldspar reactions. The main compositions and structure of precipitants were investigated from the analysis of SEM and EDS.

5.3.1 Precipitant created by the supercritical CO₂-water-plagioclase reaction

Fig. 33 shows the precipitant created from the supercritical CO₂-water-plagioclase reaction. From EDS analysis, the precipitant was mostly composed of an amorphous silicate mineral including a high content of Ca²⁺ (Table 5).

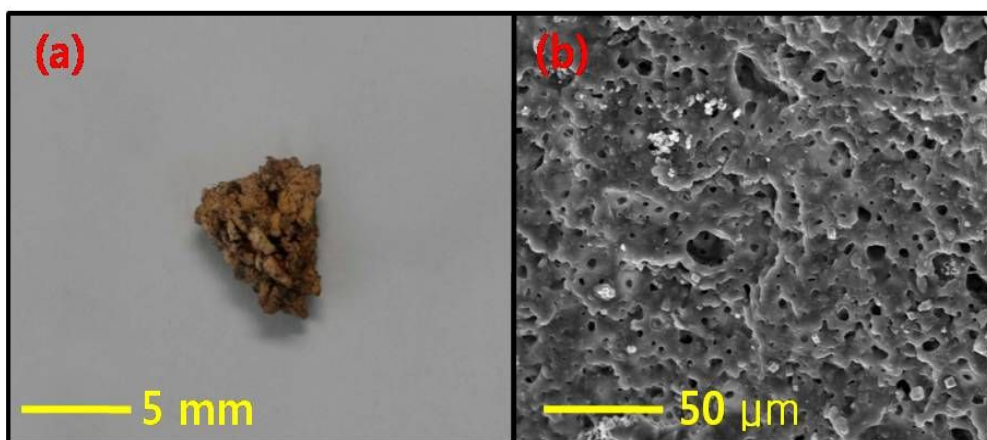


Fig. 33. Images of the precipitant created from the supercritical CO₂-water- plagioclase reaction ((a)the photograph of a precipitant and (b)SEM image of the precipitant).

Table 5. Result of the principle component analysis by EDS for the precipitant created from the supercritical CO₂-water-plagioclase reaction

Element	Atomic (%)	Weight (%)
O	51.05	34.16
Al	0.28	0.31
Si	35.75	42.00
Ca	8.90	14.92
Ti	2.42	4.85
Fe	1.61	3.76
Total	100.00	100.00

5.3.2 Precipitant created by the supercritical CO₂-water-orthoclase reaction

Fig. 34 shows the precipitants created from the supercritical CO₂-water-orthoclase reaction in the cell at 100 bar and 50 °C. From EDS analysis, precipitants consisted mainly of O²⁻, Al³⁺, and Si⁴⁺ and its chemical compounds were very similar to that of kaolinite (Table 6).

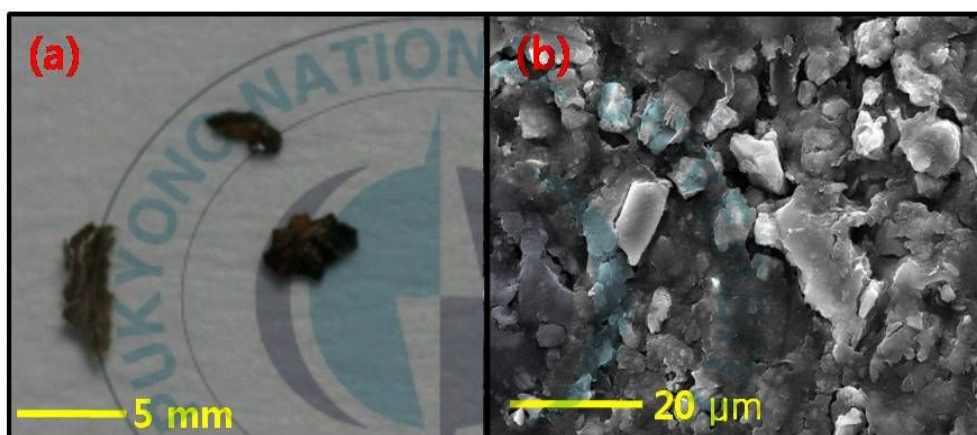


Fig. 34. Images of the precipitation created from the supercritical CO₂-water-orthoclase reaction ((a)the photograph of precipitants and (b)SEM image of the precipitants).

Table 6. Result of the principle component analysis by EDS for the precipitant created from supercritical CO₂-water-orthoclase reaction

Element	Atomic (%)	Weight (%)
O	60.31	47.07
Na	0.29	0.32
Mg	0.22	0.26
Al	30.81	40.55
Si	7.73	10.59
Cl	0.21	0.36
K	0.30	0.57
Ca	0.14	0.27
Total	100.00	100.00

The mixing of CO₂ and water in the pore system of the reservoir rock will create dissolved CO₂, carbonate ion, and/or bicarbonate ion (Gunter et al, 2000; Czernichowski-Lauriol et al, 1996). The acidification of the pore water reduces the amount of CO₂ that can be dissolved. As a consequence, rocks that buffer the pore water pH to higher values facilitate the storage of CO₂ as a dissolved phase. The CO₂-rich water may react with minerals in the reservoir rock (or caprock matrix) or with the primary pore fluid. Such reactions may cause either mineral dissolution and potential breakdown of the rock matrix or mineral precipitation and plugging of the pore system (IPCC, 2005). More sophisticated and quantified

simulations, based on laboratory experimental data derived from the use of reservoir and caprock samples and native pore fluids, are necessary to fully assess the potential effects of such reactions in more complex systems (Bachu et al, 1994; Rochelle et al, 1999). Supplementary experiments have been going to investigate more quantitatively the reaction mechanism of supercritical CO₂-mineral-brine water.



CHAPTER VI. CONCLUSION

The objective of this study is to investigate the dissolution and the re-precipitation of plagioclase ($[\text{Ca}, \text{Na}_2]\text{O} \cdot \text{Al}_2\text{O}_3 \cdot 2\text{SiO}_2$), orthoclase (KAlSi_3O_8), and biotite ($\text{K}[\text{Mg}, \text{Fe}]_3\text{AlSi}_3\text{O}_{10}(\text{OH})_2$) when the mineral reacts with supercritical CO_2 and water at the CO_2 sequestration site. For this study, the experiments of supercritical CO_2 -water-mineral were performed in high pressurized cell. The following conclusions were derived from this research;

1. Images of three phases for CO_2 obtained from the transparent window in the cell showed the distinct differences among the gaseous carbon dioxide, the liquid carbon dioxide, and the supercritical carbon dioxide. Experimental results for CO_2 phases created in the cell at different pressure and temperature conditions were matched with those from theoretical calculation, suggesting that the high pressurized cell system is available to reproduce the geochemical reactions occurred in the subsurface for CO_2 sequestration.

2. For the experiment of the supercritical CO_2 -water-plagioclase reaction, the average roughness value of the plagioclase surface was roughly changed from 0.155 nm to 2.493 nm by the mineral dissolution for 30 days of reaction. Particularly, the average roughness value dramatically increased up to more than 19 times for

the last 10 days. It was suggested that the plagioclase could be seriously weathered within several months when it comes into contact with the supercritical CO₂ and water at CO₂ sequestration site.

For the supercritical CO₂-water-orthoclase reaction, the surface of orthoclase was roughly changed by the dissolution for 30 days. The average roughness value of the orthoclase surface was 0.372 nm and it gradually increased to 1.141 nm after 20 days of the reaction. For the next 10 days, the average roughness increased considerably to 2.849 nm (about 8 times increase). This result also investigated that the orthoclase could be seriously weathered within several months when it comes into contact with the supercritical CO₂ and water.

For the experiment with biotite, the initial average roughness value was 0.659 nm, but it gradually increased to 1.097 nm after 30 days, indicating that the biotite could be weathered when it comes into contact with the supercritical CO₂-water and the amount of surface change for the biotite was lower than those of feldspars.

3. Results of the solution analysis for three minerals (plagioclase, orthoclase, and biotite) at different reaction time showed that the pH of water decreased from 8 to 4 within 10 days as the supercritical CO₂ was dissolved in the solution and it maintained around pH 4 for the whole experiment. The dissolution of Ca²⁺ from the plagioclase linearly increased with the increase of the reaction time and concentrations of Ca²⁺ and Na⁺ were 75 mg/L and 50

mg/L, respectively. Results suggested that Ca^{2+} -rich plagioclase would be significantly weathered when it contact with the supercritical CO_2 and water at CO_2 sequestration sites. For the orthoclase included high K^+ content, Al^{3+} , Ca^{2+} , and Na^+ were dissolved in order of their concentration, which were lower than 3 mg/L. Concentrations of K^+ and Si^{4+} from the orthoclase were lower than 0.5 mg/L, suggesting that the dissolution of orthoclase would be dependant on Ca^{2+} and Na^+ rather than K^+ . For a biotite, Na^+ , K^+ , Ca^{2+} , Al^{3+} , Si^{4+} , and Mg^{2+} were dissolved from the biotite in order of their concentration and concentrations of Na^+ , K^+ , and Ca^{2+} higher than 5 mg/L, suggesting that the main elements dissolved from the biotite were not Mg^{2+} , Si^{4+} , and Al^{3+} but Na^+ , K^+ , and Ca^{2+} when it contacted with the supercritical CO_2 and water.

4. The re-precipitation from dissolved ions in the high-pressurized cell occurred in the supercritical CO_2 -water-feldspar reactions (except the reaction with biotite). From SEM and EDS spectra analyses of the precipitants in the supercritical CO_2 -water-plagioclase reaction, the precipitants were mostly composed of the amorphous silicate minerals including a high content of Ca^{2+} . In case of orthoclase, the precipitants consisted mainly of O^{2-} , Al^{3+} , and Si^{4+} . Its chemical structure was very similar to that of a kaolinite. Results suggested that the process of dissolution/re-precipitation of minerals repeatedly occurs in the CO_2 sequestration site and also might change the properties of the pore spaces in the brine aquifer.

5. Limitation of our results are probably related to several factors such as irregular mineral structure, artificial brine water, and uncountable mass balance. The quantified measurement for the amount of ions dissolved from the mineral and the use of genuine brine water in the experiment were essential to investigate the geochemical reaction in detail and the supplementary studies are under way.



REFERENCES

Akimoto, K., Kotsubom H., Asami, T., Li, X., Uno, M., Tomoda, T. and Ohsumi, T., 2004, Evaluation of carbon dioxide sequestration in Japan with a mathematical model, *Energy*, 29, 1537–1549.

Aresta, M., Forti G., 1987, Carbon dioxide as a source of carbon, biochemical and chemical use, *Mathematical and Physical Science*, 206.

Bachu, S., W.D. Gunter and E.H. Perkins, 1994, Aquifer disposal of CO₂, hydrodynamic and mineral trapping, *Energy Conversion and Management*, 35(4), 269–279

Bachu, S., 2000, Sequestration of carbon dioxide in geological media, Criteria and approach for site selection. *Energy Conservation and Management*, 41(9), 953–970.

Bachu, S. and J.J. Adams, 2003, Sequestration of CO₂ in geological media in response to climate change, Capacity of deep saline aquifers to sequester CO₂ in solution. *Energy Conversion and Management*, 44(20), 3151–3175.

Bachu, S. and J.C. Shaw, 2003, Evaluation of the CO₂ sequestration capacity in Alberta's oil and gas reservoirs at depletion and the

effect of underlying aquifers. *Journal of Canadian Petroleum Technology*, 42(9), 51-61.

Bachu, S., Bonijoly, D., Bradshaw, J., Burruss, R., Holloway, S., Christensen, N., Mathiassen, O., 2007, CO₂ storage capacity estimation, methodology and gaps, *Int. J. Greenhouse Gas Control* 1, 430-443.

Choi, B., Chae G., Kim, K., Koh, Y., Yun, S., 2009, Application of conceptual reactive transport modeling to geologic CO₂ sequestration, *Journal of the Geological Society of Korea*, 45(1), 55-67.

Choi, W., Kang, H., Kim, J., Lee, J., Lee, M., 2009, Study for the geochemical reaction of feldspar with supercritical CO₂ in the brine aquifer for CO₂ sequestration, *Korea Society of Economic and Environmental Geology*, 42(5), 403-412

Crowley, T.J., 2000, Causes of climate change over the past 1000 years, *Science*, 289, 270-277.

Czernichowski-Lauriol, I., B. Sanjuan, C. Rochelle, K. Bateman, J. Pearce and P. Blackwell, 1996, Analysis of the geochemical aspects of the underground disposal of CO₂, *Deep Injection Disposal of Hazardous and Industrial Wastes, Scientific and Engineering Aspects*, J.A. Apps and C.-F. Tsang (eds.), Academic Press, ISBN 0-12-060060-9, 565-583.

Emberley, S., Hutcheon, I., Shevalier, M., Durocher, K., Gunter, W.D. and Perkins, E.H., 2004, Geochemical monitoring of fluid-rock interaction at CO₂ storage at the Weyburn CO₂-injection enhanced oil recovery site, Saskatchewan, Canada, *Energy*, 29, 1393–1401.

Gale, J., N.P. Christensen, A. Cutler, and T.A. Torp, 2001, Demonstrating the Potential for Geological Storage of CO₂, The Sleipner and GESTCO Projects, *Environmental Geosciences*, 8(3), 160–65.

Gunter, W.D., E.H. Perkins and T.J. McCann, 1993, Aquifer disposal of CO₂-rich gases, reaction design for added capacity, *Energy Conversion and Management*, 34, 941–948.

Gunter, W.D., B. Wiwchar and E.H. Perkins, 1997, Aquifer disposal of CO₂-rich greenhouse gases, Extension of the time scale of experiment for CO₂-sequestering reactions by geochemical modelling, *Mineralogy and Petrology*, 59, 121–140.

Gunter, W.D., E.H. Perkins and I. Hutcheon, 2000, Aquifer disposal of acid gases, Modeling of water-rock reactions for trapping acid wastes, *Applied Geochemistry*, 15, 1085–1095.

Hitchen, B., 1996, Aquifer disposal of carbon dioxide, hydrologic and mineal trapping, Geoscience Publishing Sherwood Park, Alberta,

Canada.

Holloway, S., 1997, An overview of the underground disposal of carbon dioxide, *Energy Conversion and Management* 38, 193–198.

Houghton, J.T., Meira Filho, L.G., Griggs, D.J., Maskell, K., 1997, Stabilization of atmospheric greenhouse gases, physical, biological and socio-economic implications, International Panel for Climate Change Technical paper III.

IEA, 2003, CO₂ emissions from fuel combustion, 1971–2001, OECD/IEA, Paris.

IPCC (Intergovernmental Panel on Climate Change), 2001a, Climate Change 2001–Mitigation, The Third Assessment Report of the Intergovernmental Panel on Climate Change, Cambridge University Press, Cambridge, UK.

IPCC (Intergovernmental Panel on Climate Change), 2001b, Climate Change 2001, The Third Assessment Report of the Intergovernmental Panel on Climate Change, Cambridge University Press, Cambridge, UK.

IPCC (Intergovernmental Panel on Climate Change), 2001c, Climate Change 2001, The scientific Basis, Contribution of Working Group I to the Third Assessment Report of the Intergovernmental Panel on

Climate Change, Cambridge University Press, Cambridge, UK.

IPCC (Intergovernmental Panel on Climate Change), 2005, IPCC Special Report on Carbon Dioxide Capture and Storage, Cambridge University Press, Cambridge, UK, 208–209.

Ketzer J.M., Iglesias, R., Einloft, S., Dullius, J., Ligabue, R., de Lima, V., 2009, Water-rock- CO_2 interactions in saline aquifers aimed for carbon dioxide storage, Experimental and numerical modeling studies of the Rio Bonito Formation (Perian), southern Brazil, Applied Geochemistry, 24, 760–767.

Koide, H., Y. Tazaki, Y. Noguchi, S. Nakayama, M. Iijima, K. Ito, Y. Shindo, 1992, Subterranean containment and long-term storage of carbon dioxide in unused aquifers and in depleted natural gas reservoirs, Energy Conversion and management, 33 (5–8), 619–626.

Marchetti, C., 1977, On geo-engineering and the CO_2 problem, Climate Change, 1, 59–68.

Rochelle, C.A., J.M. Pearce and S. Holloway, 1999, The underground sequestration of carbon dioxide: containment by chemical reactions, Chemical Containment of Waste in the Geosphere, Geological Society of London Special Publication No. 157, 117–129.

Seifritz, W., 1990, CO_2 disposal by means of silicates, Nature, 345,

486.

Seifritz, W., 1992, The terrestrial storage of CO₂-ice as a means to mitigate the greenhouse effect, Hydrogen Energy Progress IX (C.D.J. Pottier and T.N. Veziroglu (eds)), 59–8.

Siddique, Q., 1990, Separation of Gases, Proceedings of 5th Priestly Conference, Roy. Soc. Chem., London, 329.

Skovholt, O., 1993, CO₂ transportation system, Energy Conversion and management, 34, 9–11, 1095–1103.

Steinberg, M. 1996: The Carnot process for CO₂ mitigation from power plants and the transportation sector. Energy Conversion and Management, 37(6), 843–48.

Salvi, S., F. Quattrocchi, M. Angelone, C.A. Brunori, A. Billi, F. Buongiorno, F. Doumaz, R. Funiciello, M. Guerra, S. Lombardi, G. Mele, L. Pizzino and F. Salvini, 2000, A multidisciplinary approach to earthquake research, implementation of a Geochemical Geographic Information System for the Gargano site, Southern Italy, Natural Hazard, 20(1), 255–278.

Streit, J., A. Siggins and B. Evans, 2005, Predicting and monitoring geomechanical effects of CO₂ injection, Carbon Dioxide Capture for Storage in Deep Geologic Formations—Results from the CO₂ Capture

Project, 2, Geologic Storage of Carbon Dioxide with Monitoring and Verification, S.M. Benson (ed.), Elsevier Science, London, 751-766.

Span, R and W. Wagner, 1996, A new equation of state for carbon dioxide covering the fluid region from the triple-point temperature to 1100K at pressures up to 800 MPa. *Journal of Phys. Chem. Data*, 25(6), 1509-1596.

United states Environmental Protection Agency (EPA), Washington; Climate change 1995

Alberta Geological Survey, Mechanisms, Means and duration of CO₂ sequestration in geochemical media.

Sorai, M., Ohsumi, T., Ishikawa, M., and Tsukamoto K., 2007, Feldspar dissolution rates mesured using phase-shift interferometry: Implications to CO₂ underground sequestration, *Applied Geochemistry*, 22, 2795-2809.

Sorai, M., Ohsumi, T., Ishikawa M., 2005, Nanoscale surface observation of feldspar dissolved under supercritical CO₂-water-mineral system, *Energy*, 30, 2334-2343.

Helgeson, H.C., Murphy, W.M., Aagaard, P., 1984, Thermodynamic and kinetic constraints on reaction rates among minerals and aqueous solutions. II. Rate constants, effective surface area, and the hydrolysis of feldspar, *Geochimica et Cosmochimica Acta*, 48(12), 2405-2432.

Nesbitt, H.W., Young, G.M., 1984, Prediction of some weathering trends of plutonic and volcanic rocks based on thermodynamic and

kinetic considerations, *Geochimica et Cosmochimica Acta*, 48(7), 1523-1534

Riddiford, F.A., Tourqui, A., Bishop, C.D., Taylor, B., Smith, M., 2003, A cleaner development: The In Salah Gas Project, Algeria, Proceedings of the 6th International Conference on Greenhouse Gas Control Technologies (GHGT-6), J. Gale and Y. Kaya, (eds.), Kyoto, Japan, 601-06.



이산화탄소 지중저장지에서 과임계이산화탄소와 물에 의한 사장석, 정장석 그리고 흑운모의 지화학적 반응 연구

최원우

부경대학교 대학원 환경지질학과

이산화탄소의 지중저장이 가능한 것으로 알려진 대염수층에서, 과임계이산화탄소 접촉에 의한 장석류와 흑운모의 지화학적 변화를 규명하기 위해 고압 셀 실험을 실시하였다. 단일 시료광물인 사장석 ($[\text{Ca}:\text{Na}_2]\text{O}\cdot\text{Al}_2\text{O}_3\cdot 2\text{SiO}_2$), 정장석 (KAlSi_3O_8) 그리고 흑운모 ($\text{K}[\text{Mg}, \text{Fe}]_3\text{AlSi}_3\text{O}_{10}(\text{OH})_2$) 슬랩을 폴리싱 한 뒤, 과임계이산화탄소를 형성하는 지중 조건을 재현할 고압 셀 내부(100 bar, 50 °C)에 고정시킨 후, 과임계이산화탄소와 30 일간 반응시켰다. 고압 셀 실험은 pH 8로 적정한 증류수(염수의 pH)를 포함한 과임계이산화탄소-물-광물 반응과 물을 제외한 과임계이산화탄소-광물 반응으로 구분하여 실시하였다. 실험 전 폴리싱이 끝난 광물시료를 대상으로 반사현미경을 통해 광물표면을 대표할 수 있는 3 지점을 선택하였고, 3 지점의 면적 ($400\ \mu\text{m}^2$, $2500\ \mu\text{m}^2$, 그리고 $10000\ \mu\text{m}^2$)에 대한 SPM 분석을 통해 실험 전 광물의 평균 거칠기 값을 측정하였다. 반응 시간에 따른 광물의 표면 변화를 규명하기 위하여, SPM (Digital Instrument, Multimode TM

SPM), ICP-OES (Perkin elmer, Optima 7000DV) 그리고 SEM/EDS (HITACHI, S-2400) 분석을 실시하여 광물 슬랩 표면의 평균 거칠기 값의 변화, 물 시료 내 용존된 이온 농도 변화, 반응 후 고압 셀 내부에 형성된 침전물 성상을 규명하였다.

과임계이산화탄소-물-광물 반응 실험 결과 사장석 표면의 평균 거칠기 값이 실험 전에는 0.118 nm 에서 반응 30 일 후에는 2.493 nm 로 약 20 배 이상 증가하였으며, 정장석 표면의 경우에도 표면 평균 거칠기 값은 0.372 nm 에서 2.849 nm 로 약 8 배 증가하였다. 흑운모의 경우에는 실험 전에 표면의 평균 거칠기가 0.659 nm 였지만, 30 일경과 후에는 1.097 nm 로 증가하였다. 이러한 표면 거칠기 변화는 SPM 이미지 사진에서도 관찰되어, 지중 대수층의 광물은 지중 주입된 과임계이산화탄소와 공극 내 존재하는 염수와 접촉하여 수개월 이내에 용해/침전 반응이 진행될 것으로 판단되었다. 과임계이산화탄소에 의해 고압 셀 내 물 시료의 pH는 실험실시 후 10일 이내에 4로 떨어졌고, 사장석 슬랩 실험의 경우 30 일 반응 후 물 시료의 이온 농도 분석 결과 Ca^{2+} 와 Na^{+} 농도가 75 mg/L, 50 mg/L로, 가장 많이 용해되는 것으로 나타났으며, 정장석의 경우 Al^{3+} , Ca^{2+} , Na^{+} , K^{+} 순으로 용존 이온 농도가 높았다. 흑운모의 경우 Na^{+} , Ca^{2+} 가 각각 7 mg/L, 6 mg/L 로 높게 나타났다. 고압 셀 안에 침전된 고상 물질의 성분 분석결과 사장석 실험의 경우 Ca 를 다량 함유한 무정형의 규산염 물질이었으며, 정장석의 경우에는 카올리나이트가 침전됨을 알 수 있었다. 표면의 풍화가 더 많이 된 정장석보다 흑운모의 이온 농도가 높은 이유는 정장석의 반응 과정 중 침전물이 형성되는 과정에 의해 이온이 소비된 것으로 판단되었다. 장석류가 흑운모에 비해 용해가 많이 된 것은 흑운모에 함유된 Mg^{2+} 와 Fe^{2+} 보다 장석류에 함유된 Ca^{2+} , K^{+} , 그리고 Na^{+} 의 용해도가 더 높기 때문이라고 판단되었다. 염수를 제외한 과임계이산화탄소와 광물만을 반응 시킨 셀 실험의 경우에는 반응 시간에 따른 광물 표면의 평균 거칠기 값의

변화나 광물 표면의 용해현상도 거의 나타나지 않아, 물이 없는 환경에서 광물과 과임계이산화탄소와의 반응에 의한 광물의 상변화 정도는 현저하게 낮을 것으로 판단되었다.

주요어: 과임계이산화탄소, 지중저장, 광물 풍화, 지 화학 반응, 대염수층



감사의 글

먼저 이 논문이 완성되기까지 많은 관심과 격려로 늘 변함없이 따뜻하게 지도해 주신 이민희 교수님께 진심으로 감사드립니다. 바쁘신 가운데 열과 성의로 논문 심사를 해주신 왕수균 교수님, 황덕홍 박사님께도 감사드립니다. 그리고 학과 박맹언 교수님, 정상용 교수님, 박계현 교수님, 백인성 교수님, 송용선 교수님, 김영석 교수님, 강태섭 교수님께도 감사드립니다.

힘들 때 마다 위로와 질책해 주셨던 성규열 박사님, 강동환 박사님, 태형선배, 필근선배, 남훈선배, 광민선배, 의준형, 태호형, 문호형, 상건형, 성일형, 호일, 진혁, 숙주, 승현, 설미에게도 감사드립니다.

그리고 친정집 우리 환토방의 형기선배, 정산선배, 종철선배, 원홍선배, 현정선배, 나인선배, 경화선배, 영재선배, 예선선배, 남호선배, 차원선배, 재연선배에게 감사드립니다. 언제나 함께 해준 현민형, 인수누나, 종성형, 지혜, 민준, 세은, 재정, 지영, 진영, 경배, 한철, 경임, 상희, 신지, 상중, 민호, 수민, 하정에게 감사의 말씀을 전합니다.

제 대학생활을 함께 해온 소울메이트 휘제, 개척자 성택, 쌍태 경태와 영태, 친구같은 후배 석준 에게도 감사의 말을 전합니다. 그리고 많은 추억을 함께한 문균, 공식, 태원, 진성, 건철, 영석이 에게도 감사드립니다.

마지막으로 제가 존재하는 의미인 우리 가족들.... 아버지, 어머니, 효정이 늘 사랑하고 감사드립니다. 이제 졸업을 앞두고 사회를 나가는 문턱에 서니 설렘과 두려움이 앞섭니다. 후회 없는 삶을 살도록 노력하는 사람이 되어 은혜에 보답하겠습니다.

APPENDIX

